Determining the Dirac CP violation phase in the neutrino mixing matrix from sum rules

I. Girardi [a,*], S.T. Petcov [a,b,1], A.V. Titov [a]

[a] *SISSA/INFN, Via Bonomea 265, 34136 Trieste, Italy*
[b] *Kavli IPMU (WPI), University of Tokyo, 5-1-5 Kashiwanoha, 277-8583 Kashiwa, Japan*

Abstract

Using the fact that the neutrino mixing matrix $U = U_e^\dagger U_\nu$, where U_e and U_ν result from the diagonalisation of the charged lepton and neutrino mass matrices, we analyse the sum rules which the Dirac phase δ present in U satisfies when U_ν has a form dictated by, or associated with, discrete symmetries and U_e has a "minimal" form (in terms of angles and phases it contains) that can provide the requisite corrections to U_ν, so that reactor, atmospheric and solar neutrino mixing angles θ_{13}, θ_{23} and θ_{12} have values compatible with the current data. The following symmetry forms are considered: i) tri-bimaximal (TBM), ii) bimaximal (BM) (or corresponding to the conservation of the lepton charge $L' = L_e - L_\mu - L_\tau$ (LC)), iii) golden ratio type A (GRA), iv) golden ratio type B (GRB), and v) hexagonal (HG). We investigate the predictions for δ in the cases of TBM, BM (LC), GRA, GRB and HG forms using the exact and the leading order sum rules for $\cos\delta$ proposed in the literature, taking into account also the uncertainties in the measured values of $\sin^2\theta_{12}$, $\sin^2\theta_{23}$ and $\sin^2\theta_{13}$. This allows us, in particular, to assess the accuracy of the predictions for $\cos\delta$ based on the leading order sum rules and its dependence on the values of the indicated neutrino mixing parameters when the latter are varied in their respective 3σ experimentally allowed ranges.

* Corresponding author.
 E-mail address: igirardi@sissa.it (I. Girardi).
[1] Also at: Institute of Nuclear Research and Nuclear Energy, Bulgarian Academy of Sciences, 1784 Sofia, Bulgaria.

1. Introduction

One of the major goals of the future experimental studies in neutrino physics is the searches for CP violation (CPV) effects in neutrino oscillations (see, e.g., [1,2]). It is part of a more general and ambitious program of research aiming to determine the status of the CP symmetry in the lepton sector.

In the case of the reference 3-neutrino mixing scheme,[2] CPV effects in the flavour neutrino oscillations, i.e., a difference between the probabilities of $\nu_l \to \nu_{l'}$ and $\bar{\nu}_l \to \bar{\nu}_{l'}$ oscillations in vacuum [3,4], $P(\nu_l \to \nu_{l'})$ and $P(\bar{\nu}_l \to \bar{\nu}_{l'})$, $l \neq l' = e, \mu, \tau$, can be caused, as is well known, by the Dirac phase present in the Pontecorvo, Maki, Nakagawa and Sakata (PMNS) neutrino mixing matrix $U_{\text{PMNS}} \equiv U$. If the neutrinos with definite masses ν_i, $i = 1, 2, 3$, are Majorana particles, the 3-neutrino mixing matrix contains two additional Majorana CPV phases [4]. However, the flavour neutrino oscillation probabilities $P(\nu_l \to \nu_{l'})$ and $P(\bar{\nu}_l \to \bar{\nu}_{l'})$, $l, l' = e, \mu, \tau$, do not depend on the Majorana phases[3] [4,8]. Our interest in the CPV phases present in the neutrino mixing matrix is stimulated also by the intriguing possibility that the Dirac phase and/or the Majorana phases in U_{PMNS} can provide the CP violation necessary for the generation of the observed baryon asymmetry of the Universe [9,10].

In the standard parametrisation [1] of the PMNS matrix we are going to employ in our further discussion, U_{PMNS} is expressed in terms of the solar, atmospheric and reactor neutrino mixing angles θ_{12}, θ_{23} and θ_{13}, respectively, and the Dirac and Majorana CPV phases, as follows:

$$U = V Q, \quad Q = \text{diag}\left(1, e^{i\frac{\alpha_{21}}{2}}, e^{i\frac{\alpha_{31}}{2}}\right), \tag{1}$$

where $\alpha_{21,31}$ are the two Majorana CPV phases and V is a CKM-like matrix,

$$V = \begin{pmatrix} c_{12}c_{13} & s_{12}c_{13} & s_{13}e^{-i\delta} \\ -s_{12}c_{23} - c_{12}s_{23}s_{13}e^{i\delta} & c_{12}c_{23} - s_{12}s_{23}s_{13}e^{i\delta} & s_{23}c_{13} \\ s_{12}s_{23} - c_{12}c_{23}s_{13}e^{i\delta} & -c_{12}s_{23} - s_{12}c_{23}s_{13}e^{i\delta} & c_{23}c_{13} \end{pmatrix}. \tag{2}$$

In Eq. (2), δ is the Dirac CPV phase, $0 \leq \delta \leq 2\pi$, we have used the standard notation $c_{ij} = \cos\theta_{ij}$, $s_{ij} = \sin\theta_{ij}$, and $0 \leq \theta_{ij} \leq \pi/2$. If CP invariance holds, we have $\delta = 0, \pi, 2\pi$, the values 0 and 2π being physically indistinguishable.

The existing neutrino oscillation data allow us to determine the neutrino mixing parameters $\sin^2\theta_{12}$, $\sin^2\theta_{23}$ and $\sin^2\theta_{13}$, which are relevant for our further analysis, with a relatively good precision [11,12]. The best fit values and the 3σ allowed ranges of $\sin^2\theta_{12}$, $\sin^2\theta_{23}$ and $\sin^2\theta_{13}$, found in the global analysis in Ref. [11] read:

$$(\sin^2\theta_{12})_{\text{BF}} = 0.308, \quad 0.259 \leq \sin^2\theta_{12} \leq 0.359, \tag{3}$$

$$(\sin^2\theta_{23})_{\text{BF}} = 0.437 \, (0.455), \quad 0.374 \, (0.380) \leq \sin^2\theta_{23} \leq 0.626 \, (0.641), \tag{4}$$

$$(\sin^2\theta_{13})_{\text{BF}} = 0.0234 \, (0.0240), \quad 0.0176 \, (0.0178) \leq \sin^2\theta_{13} \leq 0.0295 \, (0.0298), \tag{5}$$

where the values (values in brackets) correspond to neutrino mass spectrum with normal ordering (inverted ordering) (see, e.g., [1]), denoted further as NO (IO) spectrum.

---

[2] All compelling data on neutrino masses, mixing and oscillations are compatible with the existence of mixing of three light neutrinos ν_i, $i = 1, 2, 3$, with masses $m_i \lesssim 1$ eV in the weak charged lepton current (see, e.g., [1]).

[3] The Majorana phases can play important role, e.g., in $|\Delta L| = 2$ processes like neutrinoless double beta $((\beta\beta)_{0\nu}$-) decay $(A, Z) \to (A, Z + 2) + e^- + e^-$, L being the total lepton charge, in which the Majorana nature of massive neutrinos ν_i, if any, manifests itself (see, e.g., [5–7]).

In the present article we will be concerned with the predictions for the Dirac phase δ and will not discuss the Majorana phases in what follows. More specifically, we will be interested in the predictions for the Dirac CPV phase δ which are based on the so-called "sum rules" for $\cos\delta$ [13–15] (see also, e.g., [16–18]). The sum rules of interest appear in an approach aiming at quantitative understanding of the pattern of neutrino mixing on the basis of symmetry considerations. In this approach one exploits the fact that, up to perturbative corrections, the PMNS matrix has an approximate form, U_ν, which can be dictated by symmetries. The matrix U_ν is assumed to originate from the diagonalisation of the neutrino Majorana mass term. The angles in U_ν have specific symmetry values which differ, in general, from the experimentally determined values of the PMNS angles θ_{12}, θ_{13} and θ_{23}, and thus need to be corrected. The requisite perturbative corrections, which modify the values of the angles in U_ν to coincide with the measured values of θ_{12}, θ_{13} and θ_{23}, are provided by the matrix U_e arising from the diagonalisation of the charged lepton mass matrix, $U = U_e^\dagger U_\nu$. In the sum rules we will analyse in detail in the present article the Dirac phase δ, more precisely, $\cos\delta$, is expressed, in general, in terms of the mixing angles θ_{12}, θ_{13} and θ_{23} of the PMNS matrix U and the angles present in U_ν, whose values are fixed, being dictated by an underlying approximate discrete symmetry of the lepton sector (see, e.g., [17]).

2. The sum rules

In the framework of the reference 3 flavour neutrino mixing we will consider, the PMNS neutrino mixing matrix is always given by

$$U = U_e^\dagger U_\nu, \tag{6}$$

where U_e and U_ν are 3×3 unitary matrices originating from the diagonalisation of the charged lepton and the neutrino (Majorana) mass terms. As we have already indicated, we will suppose in what follows that U_ν has a form which is dictated by symmetries. More specifically, we will assume that

$$U_\nu = \Psi_1 \, \tilde{U}_\nu \, Q_0 = \Psi_1 \, R_{23}\left(\theta_{23}^\nu\right) R_{12}\left(\theta_{12}^\nu\right) Q_0, \tag{7}$$

where $R_{23}(\theta_{23}^\nu)$ and $R_{12}(\theta_{12}^\nu)$ are orthogonal matrices describing rotations in the 2-3 and 1-2 planes, respectively, and Ψ_1 and Q_0 are diagonal phase matrices each containing two phases. Obviously, the phases in the matrix Q_0 give contribution to the Majorana phases in the PMNS matrix. In the present article we will consider the following symmetry forms of the matrix $\tilde{U}_\nu$: i) tri-bimaximal (TBM) [19], ii) bimaximal (BM), or due to a symmetry corresponding to the conservation of the lepton charge $L' = L_e - L_\mu - L_\tau$ (LC) [20,21], iii) golden ratio type A (GRA) form [22,23], iv) golden ratio type B (GRB) form [24], and v) hexagonal (HG) form [25,26]. The TBM, BM, GRA, GRB and HG forms can be obtained respectively from, e.g., T'/A_4, S_4, A_5, D_{10} and D_{12} discrete (lepton) flavour symmetries (see, e.g., [17,22–24,26–28]). In all these cases we have $\theta_{23}^\nu = -\pi/4$, and the matrix $\tilde{U}_\nu$ is given by

$$\tilde{U}_\nu = \begin{pmatrix} \cos\theta_{12}^\nu & \sin\theta_{12}^\nu & 0 \\ -\dfrac{\sin\theta_{12}^\nu}{\sqrt{2}} & \dfrac{\cos\theta_{12}^\nu}{\sqrt{2}} & -\dfrac{1}{\sqrt{2}} \\ -\dfrac{\sin\theta_{12}^\nu}{\sqrt{2}} & \dfrac{\cos\theta_{12}^\nu}{\sqrt{2}} & \dfrac{1}{\sqrt{2}} \end{pmatrix}. \tag{8}$$

The TBM, BM (LC), GRA, GRB and HG forms of $\tilde{U}_\nu$ correspond to different fixed values of θ_{12}^ν and thus of $\sin^2\theta_{12}^\nu$, namely, to i) $\sin^2\theta_{12}^\nu = 1/3$, ii) $\sin^2\theta_{12}^\nu = 1/2$, iii) $\sin^2\theta_{12}^\nu = (2+r)^{-1} \cong 0.276$, r being the golden ratio, $r = (1+\sqrt{5})/2$, iv) $\sin^2\theta_{12}^\nu = (3-r)/4 \cong 0.345$, and v) $\sin^2\theta_{12}^\nu = 1/4$. Thus, the matrix U_e in Eq. (6) should provide corrections which not only generate nonzero value of θ_{13}, but also lead to reactor, atmospheric and solar neutrino mixing angles θ_{13}, θ_{23} and θ_{12} which have values compatible with the current data, including a possible sizeable deviation of θ_{23} from $\pi/4$. As was shown in [13], the "minimal" form of U_e, in terms of angles and phases it contains, that can provide the requisite corrections to U_ν includes a product of two orthogonal matrices describing rotations in the 2-3 and 1-2 planes, $R_{23}(\theta_{23}^e)$ and $R_{12}(\theta_{12}^e)$, θ_{23}^e and θ_{12}^e being two (real) angles. In what follows we will adopt this minimal form of U_e. It proves convenient to cast it in the form [13]:

$$U_e = \Psi_2^\dagger \tilde{U}_e = \Psi_2^\dagger R_{23}^{-1}\left(\theta_{23}^e\right) R_{12}^{-1}\left(\theta_{12}^e\right), \tag{9}$$

where Ψ_2 is a diagonal phase matrix including two phases, and

$$R_{12}\left(\theta_{12}^e\right) = \begin{pmatrix} \cos\theta_{12}^e & \sin\theta_{12}^e & 0 \\ -\sin\theta_{12}^e & \cos\theta_{12}^e & 0 \\ 0 & 0 & 1 \end{pmatrix}, \quad R_{23}\left(\theta_{23}^e\right) = \begin{pmatrix} 1 & 0 & 0 \\ 0 & \cos\theta_{23}^e & \sin\theta_{23}^e \\ 0 & -\sin\theta_{23}^e & \cos\theta_{23}^e \end{pmatrix}. \tag{10}$$

Thus, the PMNS matrix in the approach we are following is given by

$$U = U_e^\dagger U_\nu = R_{12}\left(\theta_{12}^e\right) R_{23}\left(\theta_{23}^e\right) \Psi R_{23}\left(\theta_{23}^\nu\right) R_{12}\left(\theta_{12}^\nu\right) Q_0,$$
$$\Psi = \Psi_2 \Psi_1, \quad \theta_{23}^\nu = -\frac{\pi}{4}. \tag{11}$$

The matrices Ψ and Q_0 are diagonal phase matrices each containing, in general, two physical CPV phases[4] [29]:

$$\Psi = \mathrm{diag}\left(1, e^{-i\psi}, e^{-i\omega}\right), \quad Q_0 = \mathrm{diag}\left(1, e^{i\frac{\xi_{21}}{2}}, e^{i\frac{\xi_{31}}{2}}\right). \tag{12}$$

As was explained earlier, the requirement that U_e has a "minimal" form in terms of angles and phases it contains, needed to provide the requisite corrections to U_ν, makes not necessary the inclusion in $\tilde{U}_e$ of the orthogonal matrix describing the rotation in the 1-3 plane, $R_{13}(\theta_{13}^e)$. Effectively, this is equivalent to the assumption that the angle θ_{13}^e, if nonzero, is sufficiently small and thus is either negligible, or leads to sub-dominant effects in the observable of interest in the present analysis, $\cos\delta$. We will use $\theta_{13}^e \cong 0$ to denote values of θ_{13}^e which satisfy the indicated condition.

We note that $\theta_{13}^e \cong 0$ is a feature of many theories of charged lepton and neutrino mass generation (see, e.g., [22,27,28,30–32]). The assumption that $\theta_{13}^e \cong 0$ was also used in a large number of studies dedicated to the problem of understanding the origins of the observed pattern of lepton mixing (see, e.g., [15,29,33–37]). In large class of GUT inspired models of flavour, the matrix U_e is directly related to the quark mixing matrix (see, e.g., [28,30,31,38]). As a consequence, in this class of models we have $\theta_{13}^e \cong 0$. We will comment later on the possible effects of $\theta_{13}^e \neq 0$, $|\sin\theta_{13}^e| \ll 1$, on the predictions for $\cos\delta$, which are of principal interest of the present study.

---

[4] The diagonal phase matrix Ψ, as we see, can originate from the charged lepton or the neutrino sector, or else can receive contributions from both sectors [29].

More generally, the approach to understanding the observed pattern of neutrino mixing on the basis of discrete symmetries employed in the present article, which leads to the sum rule of interest for $\cos\delta$, is by no means unique — it is one of the several possible approaches discussed in the literature on the subject (see, e.g., [18]). It is employed in a large number of phenomenological studies (see, e.g., [15,29,33–37]) as well as in a class of models (see, e.g., [27,28,30,31,38]) of neutrino mixing based on discrete symmetries. However, it should be clear that the conditions which define the approach used in the present article are not fulfilled in all models with discrete flavour symmetries. For example, they are not fulfilled in the models with discrete flavour symmetry $\Delta(6n^2)$ studied in [39,40], with the S_4 flavour symmetry constructed in [41] and in the models discussed in [42].

Following [13], we will use the following rearrangement of the product of matrices $R_{23}(\theta_{23}^e)\Psi$ $R_{23}(\theta_{23}^\nu = -\pi/4)$ in the expression Eq. (11) for U_{PMNS}:

$$R_{23}(\theta_{23}^e)\,\Psi\,R_{23}(\theta_{23}^\nu = -\pi/4) = P_1\,\Phi\,R_{23}(\hat{\theta}_{23})\,Q_1, \tag{13}$$

where the angle $\hat{\theta}_{23}$ is determined by

$$\sin^2\hat{\theta}_{23} = \frac{1}{2}\left(1 - 2\sin\theta_{23}^e\cos\theta_{23}^e\cos(\omega - \psi)\right), \tag{14}$$

and

$$P_1 = \mathrm{diag}\left(1, 1, e^{-i\alpha}\right), \quad \Phi = \mathrm{diag}\left(1, e^{i\phi}, 1\right), \quad Q_1 = \mathrm{diag}\left(1, 1, e^{i\beta}\right). \tag{15}$$

In Eq. (15)

$$\alpha = \gamma + \psi + \omega, \quad \beta = \gamma - \phi, \tag{16}$$

and

$$\gamma = \arg\left(-e^{-i\psi}\cos\theta_{23}^e + e^{-i\omega}\sin\theta_{23}^e\right), \quad \phi = \arg\left(e^{-i\psi}\cos\theta_{23}^e + e^{-i\omega}\sin\theta_{23}^e\right). \tag{17}$$

The phase α in the matrix P_1 can be absorbed in the τ lepton field and, thus, is unphysical. The phase β gives a contribution to the matrix $\hat{Q} = Q_1\,Q_0$; the diagonal phase matrix $\hat{Q}$ contributes to the matrix of physical Majorana phases. In the setting considered the PMNS matrix takes the form:

$$U_{\mathrm{PMNS}} = R_{12}(\theta_{12}^e)\,\Phi(\phi)\,R_{23}(\hat{\theta}_{23})\,R_{12}(\theta_{12}^\nu)\,\hat{Q}, \tag{18}$$

where θ_{12}^ν has a fixed value which depends on the symmetry form of $\tilde{U}_\nu$ used. For the angles θ_{13}, θ_{23} and θ_{12} of the standard parametrisation of the PMNS matrix U we get in terms of the parameters in the expression Eq. (18) for U [13]:

$$\sin\theta_{13} = |U_{e3}| = \sin\theta_{12}^e\sin\hat{\theta}_{23}, \tag{19}$$

$$\sin^2\theta_{23} = \frac{|U_{\mu3}|^2}{1 - |U_{e3}|^2} = \sin^2\hat{\theta}_{23}\frac{\cos^2\theta_{12}^e}{1 - \sin^2\theta_{12}^e\sin^2\hat{\theta}_{23}} = \frac{\sin^2\hat{\theta}_{23} - \sin^2\theta_{13}}{1 - \sin^2\theta_{13}}, \tag{20}$$

$$\sin^2\theta_{12} = \frac{|U_{e2}|^2}{1 - |U_{e3}|^2} = \left(1 - \cos^2\theta_{23}\cos^2\theta_{13}\right)^{-1}\left[\sin^2\theta_{12}^\nu\sin^2\theta_{23}\right.$$
$$\left. + \cos^2\theta_{12}^\nu\cos^2\theta_{23}\sin^2\theta_{13} + \frac{1}{2}\sin2\theta_{12}^\nu\sin2\theta_{23}\sin\theta_{13}\cos\phi\right], \tag{21}$$

where Eq. (19) was used in order to obtain the expression for $\sin^2\theta_{23}$ in terms of $\hat{\theta}_{23}$ and θ_{13}, and Eqs. (19) and (20) were used to get the last expression for $\sin^2\theta_{12}$. Within the approach employed, the expressions in Eqs. (19)–(21) are exact.

It follows from Eqs. (1), (2) and (18) that the four observables θ_{12}, θ_{23}, θ_{13} and δ are functions of three parameters θ_{12}^e, $\hat{\theta}_{23}$ and ϕ. As a consequence, the Dirac phase δ can be expressed as a function of the three PMNS angles θ_{12}, θ_{23} and θ_{13} [13], leading to a new "sum rule" relating δ and θ_{12}, θ_{23} and θ_{13}. For an arbitrary fixed value of the angle θ_{12}^ν the sum rule for $\cos\delta$ reads [14]:

$$\cos\delta = \frac{\tan\theta_{23}}{\sin 2\theta_{12}\sin\theta_{13}}\left[\cos 2\theta_{12}^\nu + \left(\sin^2\theta_{12} - \cos^2\theta_{12}^\nu\right)\left(1 - \cot^2\theta_{23}\sin^2\theta_{13}\right)\right]. \quad (22)$$

For $\theta_{12}^\nu = \pi/4$ and $\theta_{12}^\nu = \sin^{-1}(1/\sqrt{3})$ the expression Eq. (22) for $\cos\delta$ reduces to those found in [13] in the BM (LC) and TBM cases, respectively. A similar sum rule for an arbitrary θ_{12}^ν can be derived for the phase ϕ [13,14]. It proves convenient for our further discussion to cast the sum rules for $\cos\delta$ and $\cos\phi$ of interest in the form:

$$\sin^2\theta_{12} = \cos^2\theta_{12}^\nu + \frac{\sin 2\theta_{12}\sin\theta_{13}\cos\delta - \tan\theta_{23}\cos 2\theta_{12}^\nu}{\tan\theta_{23}(1 - \cot^2\theta_{23}\sin^2\theta_{13})}, \quad (23)$$

$$\sin^2\theta_{12} = \cos^2\theta_{12}^\nu + \frac{1}{2}\sin 2\theta_{23}\frac{\sin 2\theta_{12}^\nu\sin\theta_{13}\cos\phi - \tan\theta_{23}\cos 2\theta_{12}^\nu}{(1 - \cos^2\theta_{23}\cos^2\theta_{13})}. \quad (24)$$

The phases δ and ϕ are related by [14]:

$$\sin\delta = -\frac{\sin 2\theta_{12}^\nu}{\sin 2\theta_{12}}\sin\phi, \quad (25)$$

$$\cos\delta = \frac{\sin 2\theta_{12}^\nu}{\sin 2\theta_{12}}\cos\phi\left(-1 + \frac{2\sin^2\theta_{23}}{\sin^2\theta_{23}\cos^2\theta_{13} + \sin^2\theta_{13}}\right)$$
$$+ \frac{\cos 2\theta_{12}^\nu}{\sin 2\theta_{12}}\frac{\sin 2\theta_{23}\sin\theta_{13}}{\sin^2\theta_{23}\cos^2\theta_{13} + \sin^2\theta_{13}}. \quad (26)$$

Within the scheme considered the sum rules Eqs. (22)–(24) and the relations Eqs. (25) and (26) are exact. In a complete self-consistent theory of (lepton) flavour based on discrete flavour symmetry, the indicated sum rules and relations are expected to get corrections due to, e.g., $\theta_{13}^e \neq 0$, renormalisation group (RG) effects, etc. Analytic expression for the correction in the expression for $\cos\delta$, Eq. (22), due to $|\sin\theta_{13}^e| \ll 1$ was derived in [14]. As was shown in [14], for the best fit values of the lepton mixing angles θ_{12}, θ_{13} and θ_{23}, a nonzero $\theta_{13}^e \lesssim 10^{-3}$ produces a correction to the value of $\cos\delta$ obtained from the "exact" sum rule Eq. (22), which does not exceed 11% (4.9%) in the TBM (GRB) cases and is even smaller in the other three cases of symmetry forms of $\tilde{U}_\nu$ analysed in the present article. A value of $\theta_{13}^e \lesssim 10^{-3}$ is a feature of many theories and models of charged lepton and neutrino mass generation (see, e.g., [22,27,28,30–32]). The RG effects on the lepton mixing angles and the CPV phases are known to be negligible for hierarchical neutrino mass spectrum (see, e.g., [43,44] and the references quoted therein); these effects are relatively small for values of the lightest neutrino mass not exceeding approximately 0.05 eV.[5] We will call the sum rules and the relations given in

---

Eqs. (22)–(24), (25) and (26) "exact", keeping in mind that they can be subject to corrections, which, however, in a number of physically interesting cases, if not absent, can only be sub-dominant.

A parametrisation of the PMNS matrix, similar to that given in Eq. (11), has been effectively employed in Ref. [15]: the hierarchy of values of the angles in the matrices U_e and U_ν assumed in [15] leads the authors to consider the angles θ_{13}^e and θ_{13}^ν of the 1-3 rotations in U_e and U_ν as negligibly small. As a consequence, the PMNS matrix is effectively parametrised in [15] with four angles θ_{12}^e, θ_{23}^e, θ_{12}^ν, θ_{23}^ν and[6] four phases δ_{12}^e, δ_{23}^e, δ_{12}^ν, δ_{23}^ν. As is shown in Appendix A (see also Ref. [14]), these phases are related to the phases ψ, ω, ξ_{21} and ξ_{31} present in the parametrisation in Eq. (11) as follows:

$$\psi = \delta_{12}^e - \delta_{12}^\nu + \pi, \quad \omega = \delta_{23}^e + \delta_{12}^e - \delta_{23}^\nu - \delta_{12}^\nu, \tag{27}$$

$$\xi_{21} = -2\delta_{12}^\nu, \quad \xi_{31} = -2(\delta_{12}^\nu + \delta_{23}^\nu). \tag{28}$$

Treating $\sin\theta_{12}^e$ and $\sin\theta_{23}^e$ as small parameters, $|\sin\theta_{12}^e| \ll 1$, $|\sin\theta_{23}^e| \ll 1$, neglecting terms of order of, or smaller than, $O((\theta_{12}^e)^2)$, $O((\theta_{23}^e)^2)$ and $O(\theta_{12}^e\theta_{23}^e)$, and taking into account that in this approximation we have $\sin\theta_{12}^e = \sqrt{2}\sin\theta_{13}$, the following "leading order" sum rule was obtained in [15]:

$$\theta_{12} \cong \theta_{12}^\nu + \theta_{13}\cos\delta. \tag{29}$$

This sum rule can be derived from the sum rule

$$\sin\theta_{12} \cong \sin\theta_{12}^\nu + \frac{\sin 2\theta_{12}^\nu}{2\sin\theta_{12}^\nu}\sin\theta_{13}\cos\delta, \tag{30}$$

by treating $\sin 2\theta_{12}^\nu \sin\theta_{13}\cos\delta \cong \sin 2\theta_{12}^\nu \theta_{13}\cos\delta$ as a small parameter and using the Taylor expansion $\sin^{-1}(a + bx) \cong \sin^{-1}(a) + bx/\sqrt{1-a^2}$, valid for $|bx| \ll 1$.

From Eqs. (23) and (24), employing the approximations used in Ref. [15], we get:

$$\sin^2\theta_{12} \cong \sin^2\theta_{12}^\nu + \sin 2\theta_{12}\sin\theta_{13}\cos\delta, \tag{31}$$

$$\sin^2\theta_{12} \cong \sin^2\theta_{12}^\nu + \sin 2\theta_{12}^\nu \sin\theta_{13}\cos\phi. \tag{32}$$

The first equation leads (in the leading order approximation used to derive it and using $\sin 2\theta_{12} \cong \sin 2\theta_{12}^\nu$) to Eq. (29), while from the second equation we find:

$$\sin\theta_{12} \cong \sin\theta_{12}^\nu + \frac{\sin 2\theta_{12}^\nu}{2\sin\theta_{12}^\nu}\sin\theta_{13}\cos\phi, \tag{33}$$

and correspondingly,

$$\theta_{12} \cong \theta_{12}^\nu + \theta_{13}\cos\phi. \tag{34}$$

This implies that in the leading order approximation adopted in Ref. [15] we have [14] $\cos\delta = \cos\phi$. Note, however, that the sum rules for $\cos\delta$ and $\cos\phi$ given in Eqs. (31) and (32), differ somewhat by the factors multiplying the terms $\sim \sin\theta_{13}$.

As was shown in [14], the leading order sum rule (29) leads in the cases of the TBM, GRA, GRB and HG forms of $\tilde{U}_\nu$ to largely imprecise predictions for the value of $\cos\delta$: for the best

---

[6] In contrast to $\theta_{23}^\nu = \pi/4$ employed in [15], we use $\theta_{23}^\nu = -\pi/4$. The effect of the difference in the signs of $\sin\theta_{12}^e$ and $\sin\theta_{23}^e$ utilised by us and in [15] is discussed in Appendix A.

fit values of $\sin^2\theta_{12} = 0.308$, $\sin^2\theta_{13} = 0.0234$ and $\sin^2\theta_{23} = 0.425$ used in [14], they differ approximately by factors (1.4–1.9) from the values found from the exact sum rule. The same result holds for $\cos\phi$. Moreover, the predicted values of $\cos\delta$ and $\cos\phi$ differ approximately by factors of (1.5–2.0), in contrast to the prediction $\cos\delta \cong \cos\phi$ following from the leading order sum rules. The large differences between the results for $\cos\delta$ and $\cos\phi$, obtained using the leading order and the exact sum rules, are a consequence [14] of the quantitative importance of the next-to-leading order terms which are neglected in the leading order sum rules (29)–(34). The next-to-leading order terms are significant for the TBM, GRA, GRB and HG forms of $\tilde{U}_\nu$ because in all these cases the "dominant" terms $|\theta_{12} - \theta_{12}^\nu| \sim \sin^2\theta_{13}$, or equivalently[7] $|\sin^2\theta_{12} - \sin^2\theta_{12}^\nu| \sim \sin^2\theta_{13}$. It was shown also in [14] that in the case of the BM (LC) form of $\tilde{U}_\nu$ we have $|\theta_{12} - \theta_{12}^\nu| \sim \sin\theta_{13}$ and the leading order sum rules provide rather precise predictions for $\cos\delta$ and $\cos\phi$.

The results quoted above were obtained in [14] for the best fit values of the neutrino mixing parameters $\sin^2\theta_{12}$, $\sin^2\theta_{23}$ and $\sin^2\theta_{13}$. In the present article we investigate in detail the predictions for $\cos\delta$ and $\cos\phi$ in the cases of the TBM, BM (LC), GRA, GRB and HG forms of $\tilde{U}_\nu$ using the exact sum rules given in Eqs. (23) (or (22)) and (24) and the leading order sum rules in Eqs. (31) and (32), taking into account also the uncertainties in the measured values of $\sin^2\theta_{12}$, $\sin^2\theta_{23}$ and $\sin^2\theta_{13}$. This allows us to better assess the accuracy of the predictions for $\cos\delta$ and $\cos\phi$ based on the leading order sum rules and its dependence on the values of the neutrino mixing angles. We investigate also how the predictions for $\cos\delta$ and $\cos\phi$, obtained using the exact and the leading order sum rules, vary when the PMNS neutrino mixing parameters $\sin^2\theta_{12}$, $\sin^2\theta_{23}$ and $\sin^2\theta_{13}$ are varied in their respective experimentally allowed 3σ ranges.

In what follows we will present numerical results using the values of $\sin^2\theta_{12}$, $\sin^2\theta_{23}$ and $\sin^2\theta_{13}$ quoted in Eqs. (3)–(5) and corresponding to NO spectrum of neutrino masses, unless another choice is explicitly specified. The results we obtain in the case of IO spectrum differ insignificantly from those found for NO spectrum.

3. The case of negligible θ_{23}^e

The case of negligible $\theta_{23}^e \cong 0$ was investigated by many authors (see, e.g., [15,30,34–36,45, 46]). It corresponds to a large number of theories and models of charged lepton and neutrino mass generation (see, e.g., [28,30,31,33,45]). For $\theta_{23}^e \cong 0$, the sum rules of interest given in Eqs. (23) (or (22)), (24) and in Eqs. (31), (32) were analysed in detail in Ref. [14].

In the limit of negligibly small θ_{23}^e we find from Eqs. (14), (16) and (17):

$$\sin^2\hat{\theta}_{23} = \frac{1}{2}, \ \gamma = -\psi + \pi, \ \phi = -\psi = \delta_{12}^\nu - \delta_{12}^e - \pi, \ \beta = \gamma - \phi = \pi. \tag{35}$$

The phase ω is unphysical.

In the limiting case of negligible θ_{23}^e the exact sum rules for $\cos\delta$ and $\cos\phi$ take the following form [14]:

---

[7] Note that [14] since $\cos\delta$ and $\cos\phi$ in Eqs. (29)–(34) are multiplied by $\sin\theta_{13}$, the "dominant" terms $|\theta_{12} - \theta_{12}^\nu|$ and the next-to-leading order terms $\sim \sin^2\theta_{13}$ give contributions to $\cos\delta$ and $\cos\phi$, which are both of the same order and are $\sim \sin\theta_{13}$.

$$\cos\delta = \frac{(1 - 2\sin^2\theta_{13})^{\frac{1}{2}}}{\sin 2\theta_{12}\sin\theta_{13}} \left[\cos 2\theta_{12}^\nu + \left(\sin^2\theta_{12} - \cos^2\theta_{12}^\nu \right) \frac{1 - 3\sin^2\theta_{13}}{1 - 2\sin^2\theta_{13}} \right], \tag{36}$$

$$\cos\phi = \frac{1 - \sin^2\theta_{13}}{\sin 2\theta_{12}^\nu \sin\theta_{13}(1 - 2\sin^2\theta_{13})^{\frac{1}{2}}}$$

$$\times \left[\sin^2\theta_{12} - \sin^2\theta_{12}^\nu - \cos 2\theta_{12}^\nu \frac{\sin^2\theta_{13}}{1 - \sin^2\theta_{13}} \right]. \tag{37}$$

From the above equations, to leading order in $\sin\theta_{13}$ we get:

$$\cos\delta = \frac{1}{\sin 2\theta_{12}\sin\theta_{13}} \left(\sin^2\theta_{12} - \sin^2\theta_{12}^\nu \right) + O(\sin\theta_{13}), \tag{38}$$

$$\cos\phi = \frac{1}{\sin 2\theta_{12}^\nu \sin\theta_{13}} \left(\sin^2\theta_{12} - \sin^2\theta_{12}^\nu \right) + O(\sin\theta_{13}), \tag{39}$$

or equivalently,

$$\sin^2\theta_{12} = \sin^2\theta_{12}^\nu + \sin 2\theta_{12}\sin\theta_{13}\cos\delta + O(\sin^2\theta_{13}), \tag{40}$$

$$\sin^2\theta_{12} = \sin^2\theta_{12}^\nu + \sin 2\theta_{12}^\nu \sin\theta_{13}\cos\phi + O(\sin^2\theta_{13}). \tag{41}$$

The last two equations coincide with Eqs. (31) and (32) which were derived from the exact sum rules keeping the leading order corrections in both $\sin\theta_{13}$ and $\sin\theta_{23}^e$. This implies, in particular, that the correction due to $|\sin\theta_{23}^e| \ll 1$ appears in the sum rules of interest only in the next-to-leading order terms. Casting the results obtained in a form we are going to use in our numerical analysis, we obtain:

$$\sin\theta_{12} = \sin\theta_{12}^\nu + \frac{\sin 2\theta_{12}}{2\sin\theta_{12}^\nu}\sin\theta_{13}\cos\delta + O(\sin^2\theta_{13}) \tag{42}$$

$$= \sin\theta_{12}^\nu + \frac{\sin 2\theta_{12}^\nu}{2\sin\theta_{12}^\nu}\sin\theta_{13}\cos\delta + O(\sin^2\theta_{13}), \tag{43}$$

$$\sin\theta_{12} = \sin\theta_{12}^\nu + \frac{\sin 2\theta_{12}^\nu}{2\sin\theta_{12}^\nu}\sin\theta_{13}\cos\phi + O(\sin^2\theta_{13}). \tag{44}$$

We have replaced $\sin 2\theta_{12}$ with $\sin 2\theta_{12}^\nu$ in Eq. (43), so that it corresponds to Eqs. (29) and (30). In the cases of the TBM, GRA, GRB and HG symmetry forms of $\tilde{U}_\nu$ we are considering and for the best fit value of $\sin^2\theta_{12} = 0.308$ we indeed have $|\sin\theta_{12} - \sin\theta_{12}^\nu| \sim \sin^2\theta_{13}$. Thus, if one applies consistently the approximations employed in [15], which lead to Eqs. (29)–(34) (or to Eqs. (38) and (39)), one should neglect also the difference between θ_{12} and θ_{12}^ν. This leads to $\cos\delta = \cos\phi = 0$.

In Fig. 1 we show predictions for $\cos\delta$ and $\cos\phi$ in the cases of the TBM, GRA, GRB and HG forms of the matrix $\tilde{U}_\nu$, as functions of $\sin\theta_{13}$ which is varied in the 3σ interval given in Eq. (5) and corresponding to NO neutrino mass spectrum. The predictions are obtained for the best fit value of $\sin^2\theta_{12} = 0.308$ using the exact sum rules Eqs. (36) and (37) for $\cos\delta$ (solid lines) and $\cos\phi$ (dashed lines) and the leading order sum rules Eqs. (43) and (44) (dash-dotted lines). As we see in Fig. 1, the predictions for $\cos\delta$ vary in magnitude and sign when one varies the symmetry form of $\tilde{U}_\nu$. More specifically, from the exact sum rule in Eq. (36), using the best fit value of $\sin^2\theta_{13} = 0.0234$ we get for $\cos\delta$ in the cases of the TBM, BM (LC), GRA, GRB and HG forms of $\tilde{U}_\nu$, respectively: $\cos\delta = (-0.114); (-1.29); 0.289; (-0.200); 0.476$.
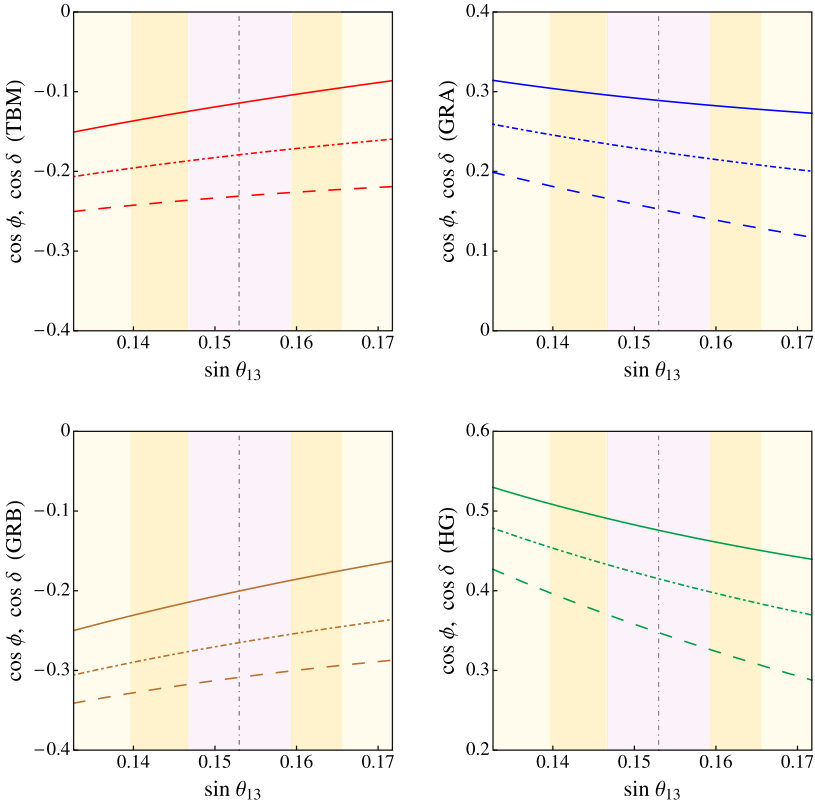
Fig. 1. Predictions for $\cos\delta$ and $\cos\phi$ in the cases of the TBM (upper left panel), GRA (upper right panel), GRB (lower left panel) and HG (lower right panel) forms of the matrix $\tilde{U}_\nu$, as functions of $\sin\theta_{13}$ and for the best fit value of $\sin^2\theta_{12} = 0.308$. The solid lines (dashed lines) correspond to $\cos\delta$ ($\cos\phi$) determined from the exact sum rule given in Eq. (36) (Eq. (37)). The dash-dotted line in each of the 4 panels represents $(\cos\delta)_{LO} = (\cos\phi)_{LO}$ obtained from the leading order sum rule in Eq. (43). The vertical dash-dotted line corresponds to the best fit value of $\sin^2\theta_{13} = 0.0234$; the three coloured vertical bands indicate the 1σ, 2σ and 3σ experimentally allowed ranges of $\sin\theta_{13}$ (see text for further details). (For interpretation of the references to colour in this figure legend, the reader is referred to the web version of this article.)

The unphysical value of $\cos\delta$ in the case of the BM (LC) form of $\tilde{U}_\nu$ is a reflection of the fact that the scheme under discussion with the BM (LC) form of the matrix $\tilde{U}_\nu$ does not provide a good description of the current data on θ_{12}, θ_{23} and θ_{13} [13]. One gets a physical result for $\cos\delta$, $\cos\delta = -0.973$, for, e.g., values of $\sin^2\theta_{12} = 0.32$, and $\sin\theta_{13} = 0.16$, lying in the 2σ experimentally allowed intervals of these neutrino mixing parameters. We have checked that for the best fit value of $\sin^2\theta_{13}$, physical values of $(\cos\delta)_E$, $(\cos\delta)_{LO}$ and $(\cos\phi)_E$ in the BM (LC) case can be obtained for relatively large values of $\sin^2\theta_{12}$. For, e.g., $\sin^2\theta_{12} = 0.359$ and $\sin^2\theta_{13} = 0.0234$ we find $(\cos\delta)_E = -0.915$, $(\cos\delta)_{LO} = -0.998$ and $(\cos\phi)_E = -0.922$. In this case the differences between the exact and leading order sum rule results for $\cos\delta$ and $\cos\phi$ are relatively small.

The above results imply that it would be possible to distinguish between the different symmetry forms of $\tilde{U}_\nu$ considered by measuring $\cos\delta$ [14], provided $\sin^2\theta_{12}$ is known with sufficiently

Table 1

The predicted values of $\cos\delta$ and $\cos\phi$, obtained from the exact sum rules in Eqs. (36) and (37), $(\cos\delta)_E$ and $(\cos\phi)_E$, and from the leading order sum rule in Eq. (43), $(\cos\delta)_{LO} = (\cos\phi)_{LO}$, using the best fit values of $\sin^2\theta_{13} = 0.0234$ and $\sin^2\theta_{12} = 0.308$, for the TBM, GRA, GRB and HG forms of the matrix $\tilde{U}_\nu$. The values of the ratios $(\cos\delta)_E/(\cos\delta)_{LO}$, $(\cos\delta)_E/(\cos\phi)_E$ and $(\cos\phi)_E/(\cos\phi)_{LO}$ are also shown.

$\sin^2\theta_{12} = 0.308$	TBM	GRA	GRB	HG
$(\cos\delta)_E$	−0.114	0.289	−0.200	0.476
$(\cos\delta)_{LO}$	−0.179	0.225	−0.265	0.415
$(\cos\delta)_E/(\cos\delta)_{LO}$	0.638	1.29	0.756	1.15
$(\cos\phi)_E$	−0.231	0.153	−0.309	0.347
$(\cos\delta)_E/(\cos\phi)_E$	0.494	1.89	0.649	1.37
$(\cos\phi)_E/(\cos\phi)_{LO}$	1.29	0.680	1.16	0.837

high precision. Even determining the sign of $\cos\delta$ will be sufficient to eliminate some of the possible symmetry forms of $\tilde{U}_\nu$.

The leading order sum rules Eqs. (43) and (44) lead to values of $\cos\delta$ and $\cos\phi$, $(\cos\delta)_{LO}$ and $(\cos\phi)_{LO}$, which coincide: $(\cos\delta)_{LO} = (\cos\phi)_{LO}$. These values differ, however, from the values obtained employing the exact sum rules: $(\cos\delta)_E \neq (\cos\delta)_{LO}$, $(\cos\phi)_E \neq (\cos\phi)_{LO}$. The exact sum rule values of $\cos\delta$ and $\cos\phi$ also differ: $(\cos\delta)_E \neq (\cos\phi)_E$. We are interested both in the predictions for the values of $(\cos\delta)_E$, $(\cos\delta)_{LO}$, $(\cos\phi)_E$ and $(\cos\phi)_{LO}$, and in the differences between the exact and the leading order sum rule predictions. In Table 1 we give the values of $(\cos\delta)_E$, $(\cos\phi)_E$, $(\cos\delta)_{LO} = (\cos\phi)_{LO}$, and of the ratios $(\cos\delta)_E/(\cos\phi)_E$, $(\cos\delta)_E/(\cos\delta)_{LO}$ and $(\cos\phi)_E/(\cos\phi)_{LO}$, calculated for the best fit values of $\sin^2\theta_{13} = 0.0234$ and $\sin^2\theta_{12} = 0.308$.

As Fig. 1 indicates, the differences $|(\cos\delta)_E - (\cos\delta)_{LO}|$ and $|(\cos\phi)_E - (\cos\phi)_{LO}|$ exhibit weak dependence on the value of $\sin\theta_{13}$ when it is varied in the 3σ interval quoted in Eq. (5). The values of $\cos\delta$, obtained using the exact sum rule Eq. (36) in the TBM, GRA, GRB and HG cases, differ from those calculated using the approximate sum rule Eq. (43) by the factors 0.638, 1.29, 0.756 and 1.15, respectively. The largest difference is found to hold in the TBM case. As was shown in [14], the correction to $(\cos\delta)_{LO}$ — the leading order sum rule result for $\cos\delta$ — is given approximately by $\cos 2\theta_{12}^\nu \sin\theta_{13}/(\sin 2\theta_{12})$. For given θ_{12}^ν, the relative magnitude of the correction depends on the magnitude of the ratio $|\sin^2\theta_{12} - \sin^2\theta_{12}^\nu|/\sin\theta_{13}$. The largest correction occurs for the symmetry form of $\tilde{U}_\nu$, for which this ratio has the smallest value. For the best fit value of $\sin^2\theta_{12}$, the smallest value of the ratio of interest corresponds to the TBM form of $\tilde{U}_\nu$ and is equal approximately to 0.166.

The absolute values of the difference $|(\cos\delta)_E - (\cos\delta)_{LO}|$ for the TBM, GRB, GRA and HG symmetry forms, as it follows from Table 1, lie in the narrow interval (0.061–0.065). These differences seem to be rather small. However, they are sufficiently large to lead to misleading results. Indeed, suppose $\cos\delta$ is measured and the value determined experimentally reads: $\cos\delta = -0.18 \pm 0.025$. If one compares this value with the value of $\cos\delta$ predicted using the leading order sum rule, $(\cos\delta)_{LO}$, one would conclude that data are compatible with the TBM form of $\tilde{U}_\nu$ and that all the other forms considered by us are ruled out. Using the prediction based on the exact sum rule, i.e., $(\cos\delta)_E$, would lead to a completely different conclusion, namely, that the data are compatible only with the GRB form of $\tilde{U}_\nu$.[8] In this hypothetical example, which is

---

[8] The same hypothetical example can be used to illustrate the significance of the difference between the exact and the leading order sum rule predictions for $\cos\delta$ also in the case of $\theta_{23}^e \neq 0$ (see Table 4).
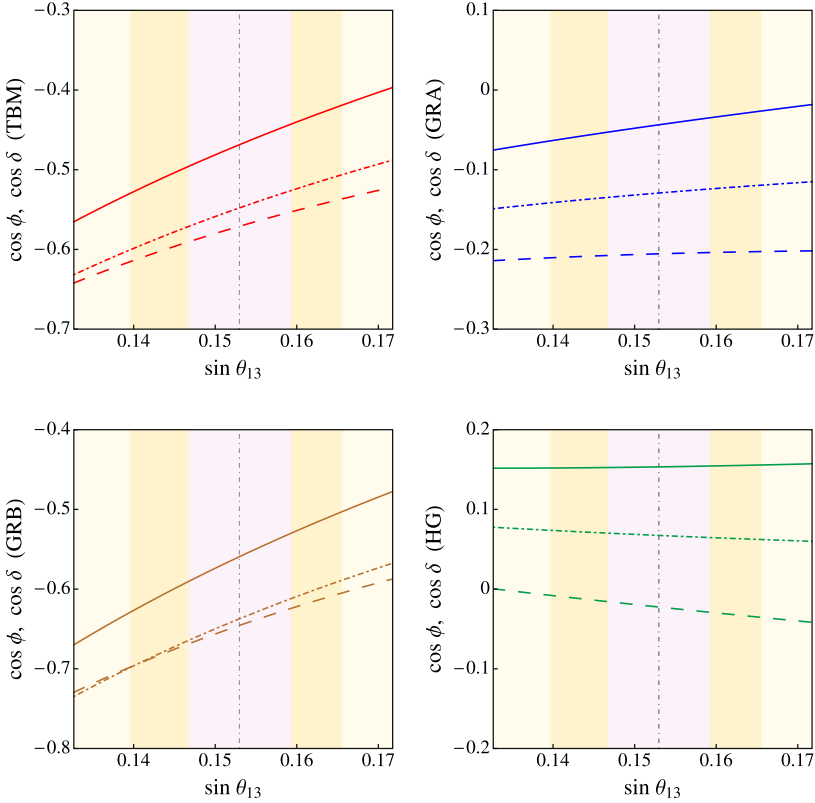
Fig. 2. The same as in Fig. 1, but for $\sin^2 \theta_{12} = 0.259$ (see text for further details).

included to illustrate the significance of the difference between the predictions for $\cos \delta$ obtained using the exact and the leading order sum rules, we have assumed that the prospective uncertainties in the predicted values of $(\cos \delta)_{LO}$ and $(\cos \delta)_E$ due to the uncertainties in the measured values of $\sin^2 \theta_{12}$, $\sin^2 \theta_{13}$ and $\sin^2 \theta_{23}$ are sufficiently small. These uncertainties will be discussed in Section 5 (see Fig. 13). The relative difference between $(\cos \delta)_E$ and $(\cos \delta)_{LO}$, i.e., the ratio $|(\cos \delta)_E - (\cos \delta)_{LO}| / |(\cos \delta)_E|$, is also significant. For the TBM, GRA, GRB and HG symmetry forms it reads: 57.0%, 22.1%, 32.5% and 12.8%, respectively.

The behaviour of $\cos \delta$ and $\cos \phi$ when $\sin \theta_{13}$ increases is determined by the sign of $(\sin^2 \theta_{12} - \sin^2 \theta_{12}^\nu)$: $\cos \delta$ and $\cos \phi$ increase (decrease) when this difference is negative (positive). For the best fit value of $\sin^2 \theta_{12} = 0.308$, this difference is negative in the TBM and GRB cases, while it is positive in the GRA and HG ones. For the four symmetry forms of $\tilde{U}_\nu$, TBM, GRB, GRA and HG, and the best fit values of $\sin^2 \theta_{13} = 0.0234$ and $\sin^2 \theta_{12} = 0.308$, the ratio $(\sin^2 \theta_{12} - \sin^2 \theta_{12}^\nu) / \sin \theta_{13}$ reads, respectively: (-0.166), (-0.245), 0.207 and 0.379.

Given the fact that the magnitude of the ratio $(\sin^2 \theta_{12} - \sin^2 \theta_{12}^\nu) / \sin \theta_{13}$ determines the factor by which $(\cos \delta)_E$ and $(\cos \delta)_{LO}$ (and $(\cos \phi)_E$ and $(\cos \phi)_{LO}$) differ, we have checked how the results described above change when $\sin^2 \theta_{12}$ is varied in its 3σ allowed region, Eq. (3). In Figs. 2 and 3 we show the dependence of the predicted values of $(\cos \delta)_E$, $(\cos \phi)_E$ and $(\cos \delta)_{LO} = (\cos \phi)_{LO}$ on $\sin \theta_{13}$ for the minimal and maximal 3σ allowed values of $\sin^2 \theta_{12}$, $\sin^2 \theta_{12} = 0.259$ and 0.359. The results shown correspond to the TBM, GRA, GRB, HG forms of $\tilde{U}_\nu$. For
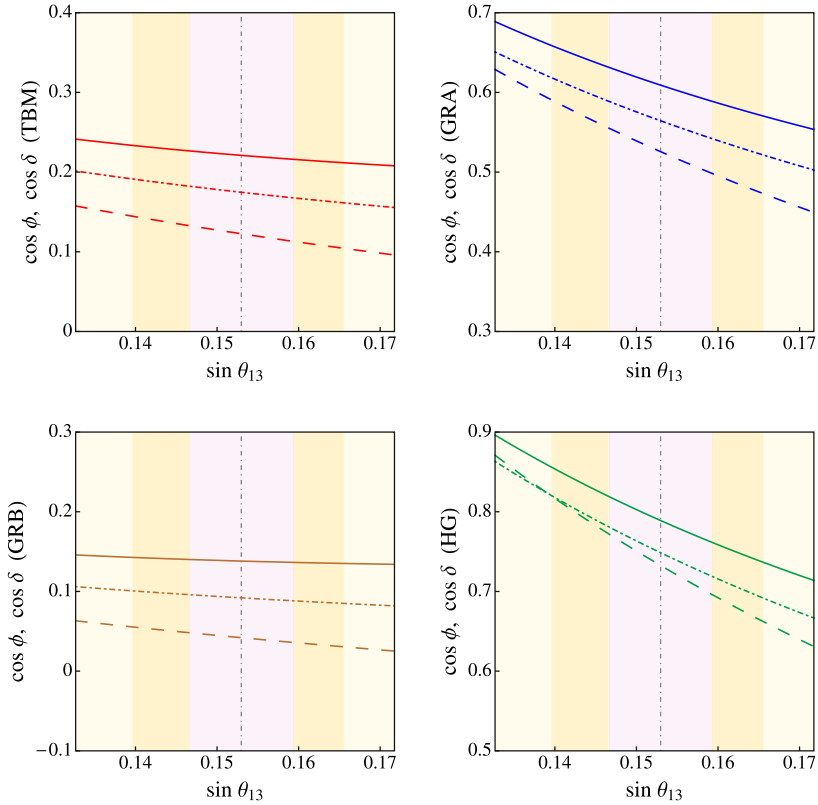
Fig. 3. The same as in Fig. 1, but for $\sin^2\theta_{12} = 0.359$ (see text for further details).

Table 2
The same as in Table 1, but for $\sin^2\theta_{12} = 0.259$.

$\sin^2\theta_{12} = 0.259$	TBM	GRA	GRB	HG
$(\cos\delta)_E$	-0.469	-0.0436	-0.559	0.153
$(\cos\delta)_{LO}$	-0.548	-0.129	-0.637	0.0673
$(\cos\delta)_E/(\cos\delta)_{LO}$	0.855	0.338	0.878	2.28
$(\cos\phi)_E$	-0.571	-0.206	-0.646	-0.0225
$(\cos\delta)_E/(\cos\phi)_E$	0.821	0.212	0.866	-6.82
$(\cos\phi)_E/(\cos\phi)_{LO}$	1.04	1.59	1.01	-0.334

$\sin^2\theta_{12} = 0.259$ ($\sin^2\theta_{12} = 0.359$) and $\sin^2\theta_{13} = 0.0234$, the ratio $(\sin^2\theta_{12} - \sin^2\theta_{12}^\nu)/\sin\theta_{13}$ in the TBM, GRA, GRB and HG cases takes respectively the values: (-0.486), (-0.114), (-0.565) and 0.059 $(0.168, 0.540, 0.088$ and $0.713)$. As in the preceding case, we give the predicted values of $(\cos\delta)_E$, $(\cos\phi)_E$, $(\cos\delta)_{LO} = (\cos\phi)_{LO}$, and the ratios between them, for $\sin^2\theta_{12} = 0.259$ ($\sin^2\theta_{12} = 0.359$) and $\sin^2\theta_{13} = 0.0234$ in Table 2 (Table 3).

It follows from the results presented in Tables 1–3 that the exact sum rule predictions of $\cos\delta$, $(\cos\delta)_E$, for the three values of $\sin^2\theta_{12} = 0.308$, 0.259 and 0.359, differ drastically. For the TBM form of $\tilde{U}_\nu$, for instance, we get, respectively, the values: $(\cos\delta)_E = (-0.114)$, (-0.469) and 0.221. For the GRA and GRB forms of $\tilde{U}_\nu$ we have, respectively, $(\cos\delta)_E = 0.289$, (-0.044),

Table 3
The same as in Table 1, but for $\sin^2\theta_{12} = 0.359$.

$\sin^2\theta_{12} = 0.359$	TBM	GRA	GRB	HG
$(\cos\delta)_E$	0.221	0.609	0.138	0.789
$(\cos\delta)_{LO}$	0.175	0.564	0.092	0.749
$(\cos\delta)_E/(\cos\delta)_{LO}$	1.27	1.08	1.50	1.05
$(\cos\phi)_E$	0.123	0.526	0.042	0.733
$(\cos\delta)_E/(\cos\phi)_E$	1.80	1.16	3.29	1.08
$(\cos\phi)_E/(\cos\phi)_{LO}$	0.702	0.931	0.456	0.979

0.609, and $(\cos\delta)_E = (-0.200), (-0.559), 0.138$. Similarly, for the HG form we find for the three values of $\sin^2\theta_{12}$: $(\cos\delta)_E = 0.476, 0.153, 0.789$. Thus, in the cases of the symmetry forms of $\tilde{U}_\nu$ considered, the exact sum rule predictions for $\cos\delta$ not only change significantly in magnitude when $\sin^2\theta_{12}$ is varied in its 3σ allowed range, but also the sign of $\cos\delta$ changes in the TBM, GRA and GRB cases (see Fig. 4).

We observe also that for $\sin^2\theta_{12} = 0.259$, the values of $\cos\delta$, obtained using the exact sum rule Eq. (36) in the TBM, GRA, GRB and HG cases differ from those calculated using the leading order sum rule in Eq. (43) by the factors 0.855, 0.338, 0.878 and 2.28, respectively; in the case of $\sin^2\theta_{12} = 0.359$ the same factors read: 1.27, 1.08, 1.50 and 1.05.

For $\sin^2\theta_{12} = 0.259$, the largest difference between the exact and leading order sum rule results for $\cos\delta$ occurs for the GRA and HG forms of $\tilde{U}_\nu$, while if $\sin^2\theta_{12} = 0.359$, the largest difference holds for the TBM and GRB forms.

As Figs. 1–3 and Tables 1–3 show, similar results are valid for $\cos\phi$ obtained from the exact and the leading order sum rules.

It is worth noting also that the values of $\cos\phi$ and $\cos\delta$, derived from the respective exact sum rules differ significantly for the TBM, GRA, GRB and HG forms of $\tilde{U}_\nu$ considered. As pointed out in [14], for the best fit values of $\sin^2\theta_{13}$ and $\sin^2\theta_{12}$ they differ by factors (1.4–2.0), as can be seen also from Table 1. This difference can be much larger for $\sin^2\theta_{12} = 0.259$ and 0.359: for these two values of $\sin^2\theta_{12}$, $\cos\delta$ and $\cos\phi$ differ in the cases of the different symmetry forms of interest approximately by factors (1.2–6.8) and (1.1–3.3), respectively.

4. The case of nonzero θ_{23}^e

For $\theta_{23}^e = 0$ we have in the scheme we are considering: $\theta_{23} \cong \pi/4 - 0.5\sin^2\theta_{13}$. A nonzero value of θ_{23}^e allows for a significant deviation of θ_{23} from $\pi/4$. Such deviation is not excluded by the current data on $\sin^2\theta_{23}$, Eq. (4): at 3σ, values of $\sin^2\theta_{23}$ in the interval (0.37–0.64) are allowed, the best fit value being $\sin^2\theta_{23} = 0.437 (0.455)$. The exact sum rules for $\cos\delta$ and $\cos\phi$, Eqs. (22), (23) and (24), depend on θ_{23}, while the leading order sum rules, Eqs. (29) and (34), are independent of θ_{23}. In this Section we are going to investigate how the dependence on θ_{23} affects the predictions for $\cos\delta$ and $\cos\phi$, based on the exact sum rules.

We note first that from the exact sum rules in Eqs. (23) and (24) we get to leading order in $\sin\theta_{13}$:

$$\sin^2\theta_{12} = \sin^2\theta_{12}^\nu + \frac{\sin 2\theta_{12}}{\tan\theta_{23}}\sin\theta_{13}\cos\delta + O(\sin^2\theta_{13}), \tag{45}$$

$$\sin^2\theta_{12} = \sin^2\theta_{12}^\nu + \frac{\sin 2\theta_{12}^\nu}{\tan\theta_{23}}\sin\theta_{13}\cos\phi + O(\sin^2\theta_{13}). \tag{46}$$
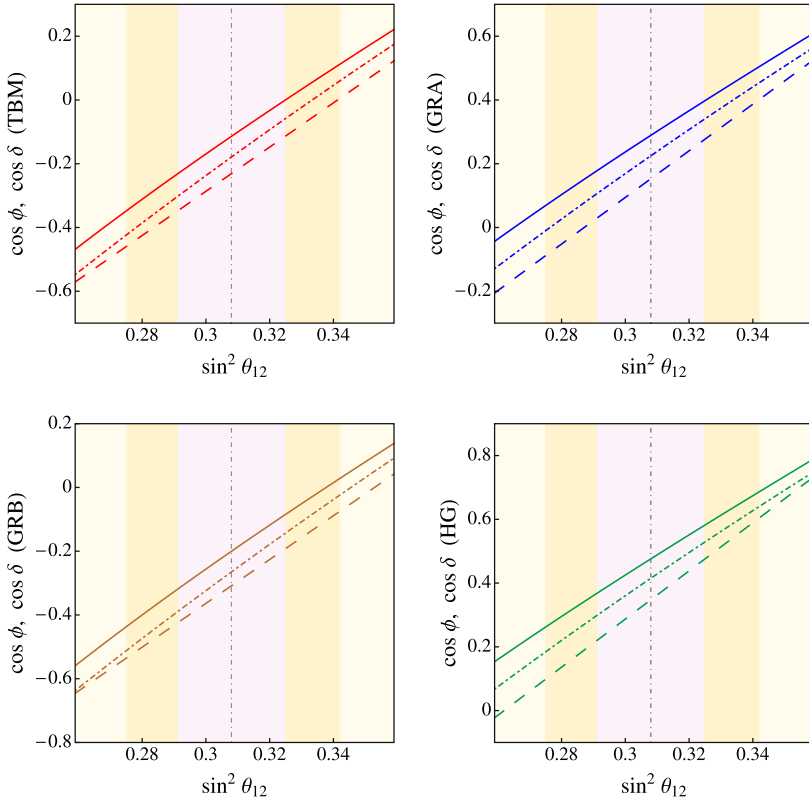
Fig. 4. The same as in Fig. 1, but for $\sin^2 \theta_{13} = 0.0234$ and varying $\sin^2 \theta_{12}$ in the 3σ range. The vertical dash-dotted line corresponds to the best fit value of $\sin^2 \theta_{12} = 0.308$ (see text for further details).

It follows from Eqs. (14) and (20) that in the case of $|\sin \theta_{23}^e| \ll 1$ considered in Ref. [15], we have [14] $(\tan \theta_{23})^{-1} \cong 2 \cos^2 \theta_{23} = 1 + O(\sin \theta_{23}^e)$. Applying the approximation employed in Ref. [15], in which terms of order of, or smaller than, $\sin^2 \theta_{13}$, $\sin^2 \theta_{23}^e$ and $\sin \theta_{13} \sin \theta_{23}^e$, in the sum rules of interest are neglected, we have to set $(\tan \theta_{23})^{-1} = 1$ in Eqs. (45) and (46). This leads to Eqs. (31) and (32) and, correspondingly, to Eqs. (29) and (34).

In Fig. 5 we show the predictions for $\cos \delta$ and $\cos \phi$ in the cases of the TBM, GRA, GRB and HG forms of the matrix $\tilde{U}_\nu$, derived from the exact sum rules in Eqs. (23) and (24), $(\cos \delta)_E$ (solid line) and $(\cos \phi)_E$ (dashed line), and from the leading order sum rule in Eq. (30) (Eq. (33)), $(\cos \delta)_{LO} = (\cos \phi)_{LO}$ (dash-dotted line). The results presented in Fig. 5 are obtained for the best fit values of $\sin^2 \theta_{12} = 0.308$ and $\sin^2 \theta_{23} = 0.437$. The parameter $\sin^2 \theta_{13}$ is varied in its 3σ allowed range, Eq. (5). In Table 4 we give the values of $(\cos \delta)_E$, $(\cos \delta)_{LO}$, $(\cos \phi)_E$ and of their ratios, corresponding to the best fit values of $\sin^2 \theta_{12}$, $\sin^2 \theta_{23}$ and $\sin^2 \theta_{13}$. We see from Table 4 that for the TBM, GRA, GRB and HG forms of $\tilde{U}_\nu$, $\cos \delta$ determined from the exact sum rule takes respectively the values (-0.091), 0.275, (-0.169) and 0.445. The values of $\cos \delta$, found using the exact sum rule, Eq. (23), differ in the TBM, GRA, GRB and HG cases from those calculated using the leading order sum rule, Eq. (30), by the factors 0.506, 1.22, 0.636 and 1.07, respectively. Thus, the largest difference between the predictions of the exact and the leading order sum rules occurs for the TBM form of $\tilde{U}_\nu$.
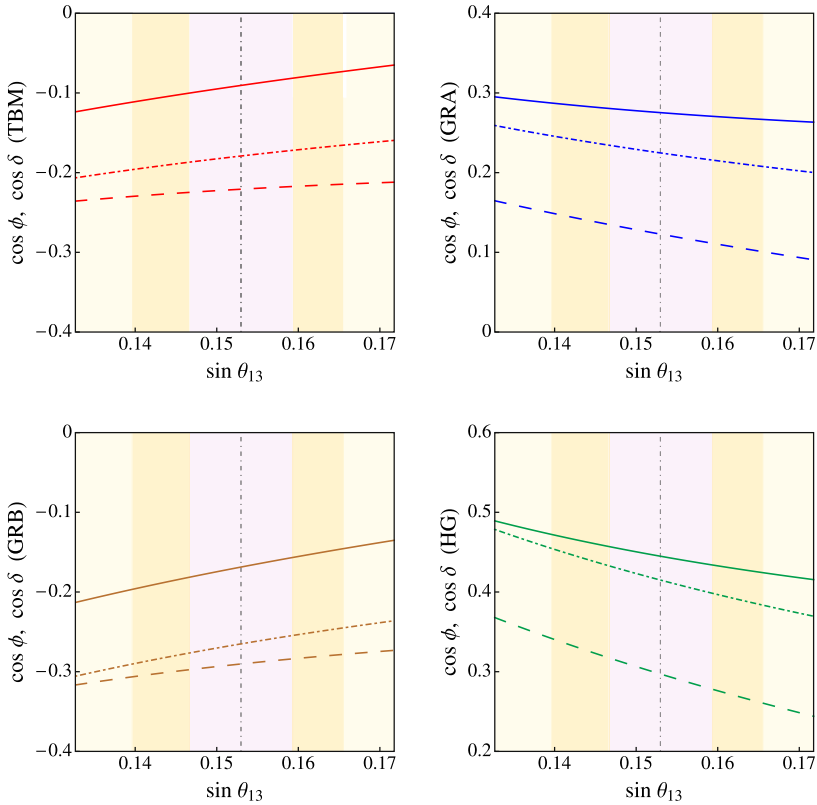
Fig. 5. Predictions for $\cos\delta$ and $\cos\phi$ in the cases of the TBM (upper left panel), GRA (upper right panel), GRB (lower left panel) and HG (lower right panel) forms of the matrix $\tilde{U}_\nu$, as functions of $\sin\theta_{13}$ and for the best fit values of $\sin^2\theta_{12} = 0.308$ and $\sin^2\theta_{23} = 0.437$. The solid lines (dashed lines) correspond to $\cos\delta$ ($\cos\phi$) determined from the exact sum rule given in Eq. (23) (Eq. (24)). The dash-dotted line in each of the 4 panels represents $(\cos\delta)_{LO} = (\cos\phi)_{LO}$ obtained from the leading order sum rule in Eq. (30) (Eq. (33)). The vertical dash-dotted line corresponds to the best fit value of $\sin^2\theta_{13} = 0.0234$; the three coloured vertical bands indicate the 1σ, 2σ and 3σ experimentally allowed ranges of $\sin\theta_{13}$ (see text for further details). (For interpretation of the references to colour in this figure legend, the reader is referred to the web version of this article.)

Table 4
The predicted values of $\cos\delta$ and $\cos\phi$, obtained from the exact sum rules in Eqs. (23) and (24), $(\cos\delta)_E$ and $(\cos\phi)_E$, and from the leading order sum rule in Eq. (30) (Eq. (33)), $(\cos\delta)_{LO} = (\cos\phi)_{LO}$, using the best fit values of $\sin^2\theta_{13} = 0.0234$, $\sin^2\theta_{12} = 0.308$ and $\sin^2\theta_{23} = 0.437$, for the TBM, GRA, GRB and HG forms of the matrix $\tilde{U}_\nu$. The values of the ratios $(\cos\delta)_E/(\cos\delta)_{LO}$, $(\cos\delta)_E/(\cos\phi)_E$ and $(\cos\phi)_E/(\cos\phi)_{LO}$ are also shown.

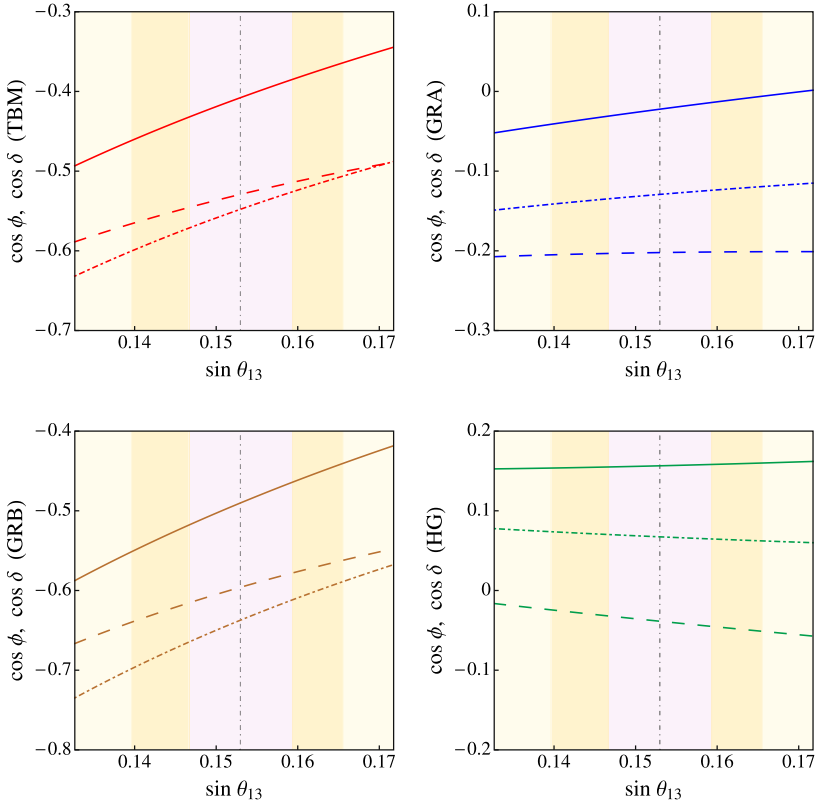| $(\sin^2\theta_{12}, \sin^2\theta_{23}) = (0.308, 0.437)$	TBM	GRA	GRB	HG
$(\cos\delta)_E$	-0.0906	0.275	-0.169	0.445
$(\cos\delta)_{LO}$	-0.179	0.225	-0.265	0.415
$(\cos\delta)_E/(\cos\delta)_{LO}$	0.506	1.22	0.636	1.07
$(\cos\phi)_E$	-0.221	0.123	-0.290	0.297
$(\cos\delta)_E/(\cos\phi)_E$	0.41	2.24	0.581	1.50
$(\cos\phi)_E/(\cos\phi)_{LO}$	1.23	0.547	1.10	0.716

Fig. 6. The same as in Fig. 5, but for $\sin^2\theta_{12} = 0.259$ (lower bound of the 3σ interval in Eq. (3)) and $\sin^2\theta_{23} = 0.437$ (best fit value).

Since the predictions of the sum rules depend on the value of θ_{12}, we show in Fig. 6 and Fig. 7 also results for the values of $\sin^2\theta_{12}$, corresponding to the lower and the upper bounds of the 3σ allowed range of $\sin^2\theta_{12}$, $\sin^2\theta_{12} = 0.259$ and 0.359, keeping $\sin^2\theta_{23}$ fixed to its best fit value. The predictions for $(\cos\delta)_E$, $(\cos\phi)_E$, $(\cos\delta)_{LO} = (\cos\phi)_{LO}$ and their ratios, obtained for the best fit values of $\sin^2\theta_{13} = 0.0234$ and $\sin^2\theta_{23} = 0.437$, and for $\sin^2\theta_{12} = 0.259$ ($\sin^2\theta_{12} = 0.359$) are given in Table 5 (Table 6). For $\sin^2\theta_{12} = 0.259$, the exact sum rule predictions of $\cos\delta$ for the TBM, GRA, GRB and HG forms of $\tilde{U}_\nu$ read (see Table 5): $(\cos\delta)_E = (-0.408)$, (-0.022), (-0.490) and 0.156. As in the case of negligible θ_{23}^e analysed in the preceding Section, these values differ drastically (in general, both in magnitude and sign) from the exact sum rule values of $\cos\delta$ corresponding to the best fit value and the 3σ upper bound of $\sin^2\theta_{12} = 0.308$ and 0.359. The dependence of $(\cos\delta)_E$, $(\cos\delta)_{LO}$ and $(\cos\phi)_E$ on $\sin^2\theta_{12}$ under discussion is shown graphically in Fig. 8.

Further, for $\sin^2\theta_{12} = 0.259$, the ratio $(\cos\delta)_E/(\cos\delta)_{LO}$ in the TBM, GRA, GRB and HG cases reads, respectively, 0.744, 0.172, 0.769 and 2.32 (see Table 5). Thus, the predictions for $\cos\delta$ of the exact and the leading order sum rules differ by the factors of 5.8 and 2.3 in the GRA and HG cases. For the upper bound of the 3σ range of $\sin^2\theta_{12} = 0.359$, the ratio $(\cos\delta)_E/(\cos\delta)_{LO}$ takes the values 1.2, 0.996, 1.46 and 0.969 for the TBM, GRA, GRB and HG
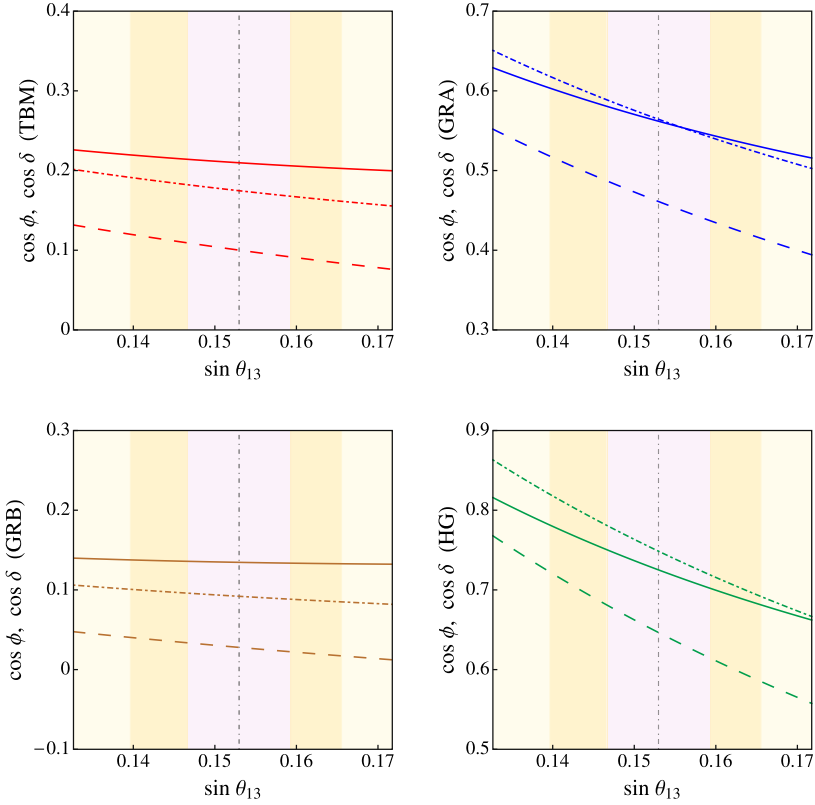
Fig. 7. The same as in Fig. 5, but for $\sin^2\theta_{12} = 0.359$ (upper bound of the 3σ interval in Eq. (3)) and $\sin^2\theta_{23} = 0.437$ (best fit value).

Table 5
The same as in Table 4, but for $\sin^2\theta_{13} = 0.0234$ (best fit value), $\sin^2\theta_{12} = 0.259$ (lower bound of the 3σ range) and $\sin^2\theta_{23} = 0.437$ (best fit value).

$(\sin^2\theta_{12}, \sin^2\theta_{23}) = (0.259, 0.437)$	TBM	GRA	GRB	HG
$(\cos\delta)_E$	-0.408	-0.0223	-0.490	0.156
$(\cos\delta)_{LO}$	-0.548	-0.129	-0.637	0.0673
$(\cos\delta)_E/(\cos\delta)_{LO}$	0.744	0.172	0.769	2.32
$(\cos\phi)_E$	-0.529	-0.202	-0.596	-0.0386
$(\cos\delta)_E/(\cos\phi)_E$	0.771	0.110	0.822	-4.05
$(\cos\phi)_E/(\cos\phi)_{LO}$	0.966	1.57	0.935	-0.573

forms of $\tilde{U}_\nu$, respectively (see Table 6). For the GRA and HG symmetry forms the leading order sum rule prediction for $\cos\delta$ is very close to the exact sum rule prediction, which can also be seen in Fig. 7.

We will investigate next the dependence of the predictions for $\cos\delta$ and $\cos\phi$ on the value of θ_{23} given the facts that i) $\sin^2\theta_{23}$ is determined experimentally with a relatively large uncertainty, and ii) in contrast to the leading order sum rule predictions for $\cos\delta$ and $\cos\phi$, the exact sum rule predictions depend on θ_{23}. In Figs. 9 and 10 we show the de-

Table 6

The same as in Table 4, but for $\sin^2\theta_{13} = 0.0234$ (best fit value), $\sin^2\theta_{12} = 0.359$ (upper bound of the 3σ range) and $\sin^2\theta_{23} = 0.437$ (best fit value).

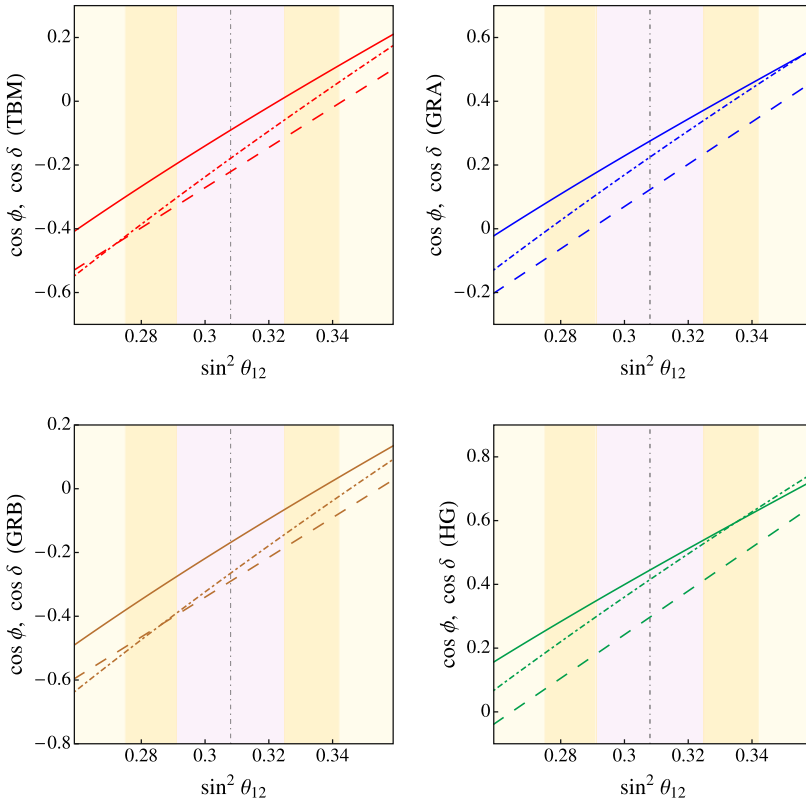| $(\sin^2\theta_{12}, \sin^2\theta_{23}) = (0.359, 0.437)$	TBM	GRA	GRB	HG
$(\cos\delta)_E$	0.210	0.562	0.135	0.725
$(\cos\delta)_{LO}$	0.175	0.564	0.092	0.749
$(\cos\delta)_E/(\cos\delta)_{LO}$	1.20	0.996	1.46	0.969
$(\cos\phi)_E$	0.100	0.461	0.0279	0.647
$(\cos\delta)_E/(\cos\phi)_E$	2.09	1.22	4.83	1.12
$(\cos\phi)_E/(\cos\phi)_{LO}$	0.573	0.817	0.303	0.864

Fig. 8. The same as in Fig. 5, but for $\sin^2\theta_{13} = 0.0234$, $\sin^2\theta_{23} = 0.437$ (best fit values) and varying $\sin^2\theta_{12}$ in the 3σ range. The vertical dash-dotted line corresponds to the best fit value of $\sin^2\theta_{12} = 0.308$.

pendence of predictions for $\cos\delta$ and $\cos\phi$ on $\sin\theta_{13}$ for the best fit value of $\sin^2\theta_{12} = 0.308$ and the 3σ lower and upper bounds of $\sin^2\theta_{23} = 0.374$ and 0.626, respectively. For $\sin^2\theta_{23} = 0.374$ (0.626) and the best fit values of $\sin^2\theta_{13}$ and $\sin^2\theta_{12}$, the exact and the leading order sum rule results $(\cos\delta)_E$, $(\cos\phi)_E$, $(\cos\delta)_{LO} = (\cos\phi)_{LO}$ and their ratios are given in Tables 7 and 8. Comparing the values of $(\cos\delta)_E$ quoted in Tables 7 and 8 with the values given in Table 4 we note that the exact sum rule predictions for $\cos\delta$ for $\sin^2\theta_{23} = 0.374$ (lower 3σ bound) and $\sin^2\theta_{23} = 0.437$ (best fit value) do not differ signif-
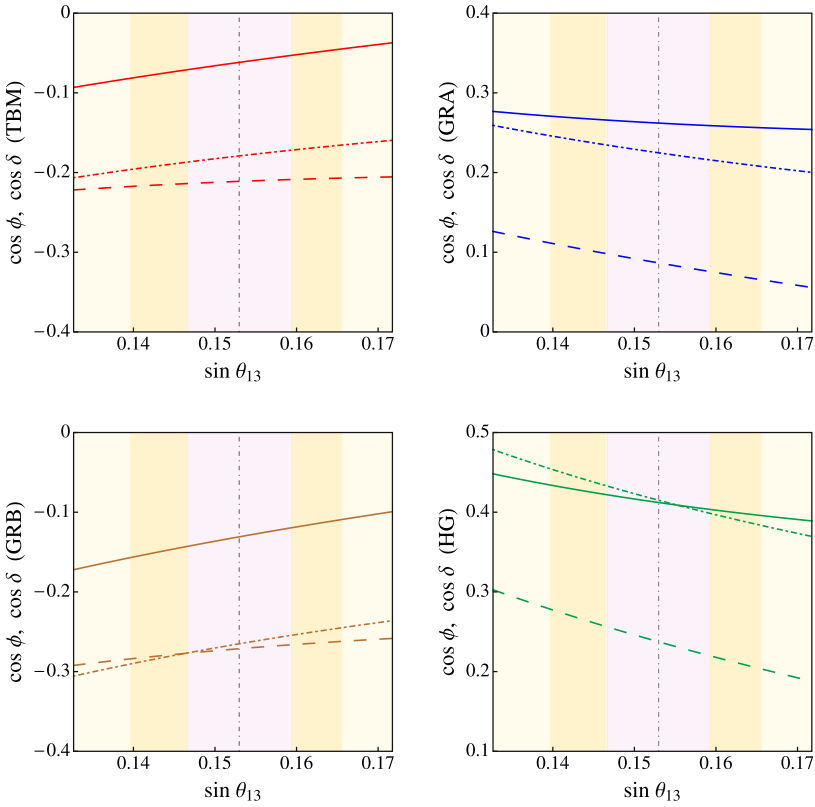
Fig. 9. The same as in Fig. 5, but for $\sin^2\theta_{12} = 0.308$ (best fit value) and $\sin^2\theta_{23} = 0.374$ (lower bound of the 3σ interval in Eq. (4)).

icantly in the cases of the TBM, GRA, GRB and HG forms of $\tilde{U}_\nu$ considered. However, the differences between the predictions for $\sin^2\theta_{23} = 0.437$ and $\sin^2\theta_{23} = 0.626$ are rather large — by factors of 2.05, 1.25, 1.77 and 1.32 in the TBM, GRA, GRB and HG cases, respectively.

In what concerns the difference between the exact and leading order sum rules predictions for $\cos\delta$, for the best fit values of $\sin^2\theta_{13}$ and $\sin^2\theta_{12}$, and for $\sin^2\theta_{23} = 0.374$, the ratio $(\cos\delta)_E/(\cos\delta)_{LO} = 0.345$, 1.17, 0.494 and 0.993 for TBM, GRA, GRB and HG forms of $\tilde{U}_\nu$. For $\sin^2\theta_{23} = 0.626$ we have for the same ratio $(\cos\delta)_E/(\cos\delta)_{LO} = 1.04$, 1.52, 1.13 and 1.42. Thus, for $\sin^2\theta_{23} = 0.374$ (0.626), the leading order sum rule prediction for $\cos\delta$ is rather precise in the HG (TBM) case. For the other symmetry forms of $\tilde{U}_\nu$ the leading order sum rule prediction for $\cos\delta$ is largely incorrect. As can be seen from Figs. 5–10 and Tables 4–8, we get similar results for $\cos\phi$.

In the case of the BM (LC) form of $\tilde{U}_\nu$, physical values of $(\cos\delta)_E$, $(\cos\phi)_E$ and $(\cos\delta)_{LO}$ can be obtained for the best fit values of $\sin^2\theta_{13}$ and $\sin^2\theta_{23}$ if $\sin^2\theta_{12}$ has a relatively large value. For, e.g., $\sin^2\theta_{12} = 0.359$, $\sin^2\theta_{13} = 0.0234$ and $\sin^2\theta_{23} = 0.437$ we find $(\cos\delta)_E = -0.821$, $(\cos\delta)_{LO} = -0.998$, $(\cos\phi)_E = -0.837$, and $(\cos\delta)_E/(\cos\delta)_{LO} = 0.823$.
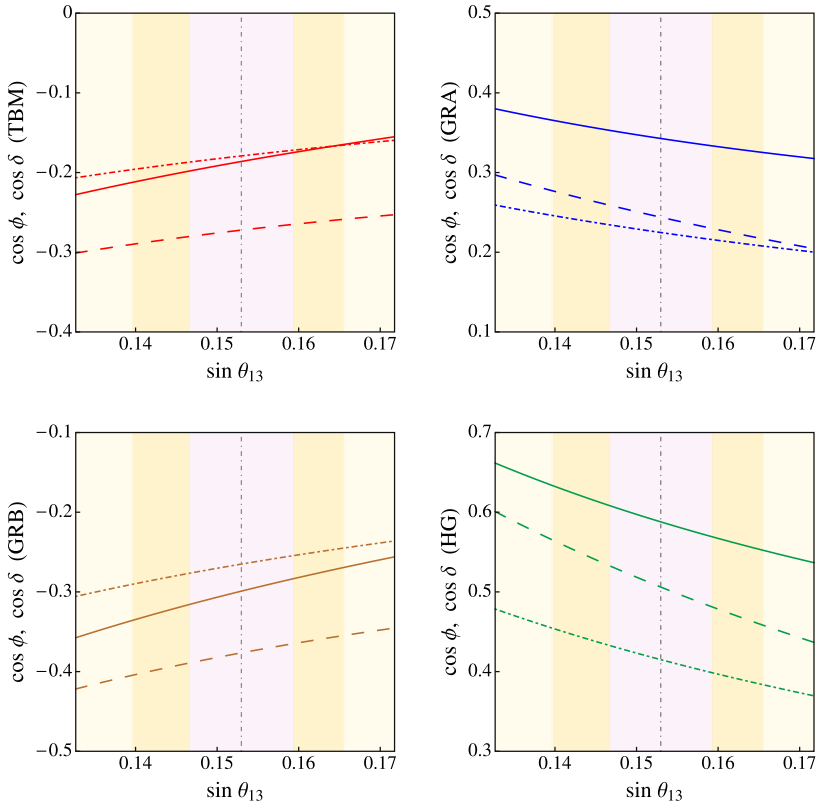
Fig. 10. The same as in Fig. 5, but for $\sin^2 \theta_{12} = 0.308$ (best fit value) and $\sin^2 \theta_{23} = 0.626$ (upper bound of the 3σ interval in Eq. (4)).

Table 7
The same as in Table 4, but for $\sin^2 \theta_{13} = 0.0234$ (best fit value), $\sin^2 \theta_{12} = 0.308$ (best fit value) and $\sin^2 \theta_{23} = 0.374$ (lower bound of the 3σ range).

$(\sin^2 \theta_{12}, \sin^2 \theta_{23}) = (0.308, 0.374)$	TBM	GRA	GRB	HG
$(\cos\delta)_{\rm E}$	-0.0618	0.262	-0.131	0.412
$(\cos\delta)_{\rm LO}$	-0.179	0.225	-0.265	0.415
$(\cos\delta)_{\rm E}/(\cos\delta)_{\rm LO}$	0.345	1.17	0.494	0.993
$(\cos\phi)_{\rm E}$	-0.211	0.0866	-0.271	0.237
$(\cos\delta)_{\rm E}/(\cos\phi)_{\rm E}$	0.293	3.03	0.483	1.74
$(\cos\phi)_{\rm E}/(\cos\phi)_{\rm LO}$	1.18	0.385	1.02	0.572

5. Statistical analysis

In the present Section we perform a statistical analysis of the predictions for δ, $\cos\delta$ and the rephasing invariant $J_{\rm CP}$ which controls the magnitude of CPV effects in neutrino oscillations [47], in the cases of the TBM, BM (LC), GRA, GRB and HG symmetry forms of the matrix $\tilde{U}_\nu$ (see Eq. (8)). In this analysis we use as input the latest results on $\sin^2 \theta_{12}$, $\sin^2 \theta_{13}$, $\sin^2 \theta_{23}$ and δ, obtained in the global analysis of the neutrino oscillation data performed in [11]. Our goal is to

Table 8

The same as in Table 4, but for $\sin^2\theta_{13} = 0.0234$ (best fit value), $\sin^2\theta_{12} = 0.308$ (best fit value) and $\sin^2\theta_{23} = 0.626$ (upper bound of the 3σ range).

$(\sin^2\theta_{12}, \sin^2\theta_{23}) = (0.308, 0.626)$	TBM	GRA	GRB	HG
$(\cos\delta)_E$	−0.186	0.343	−0.299	0.588
$(\cos\delta)_{LO}$	−0.179	0.225	−0.265	0.415
$(\cos\delta)_E/(\cos\delta)_{LO}$	1.04	1.52	1.13	1.42
$(\cos\phi)_E$	−0.272	0.244	−0.376	0.506
$(\cos\delta)_E/(\cos\phi)_E$	0.684	1.41	0.794	1.16
$(\cos\phi)_E/(\cos\phi)_{LO}$	1.52	1.09	1.42	1.22

derive the allowed ranges for δ, $\cos\delta$ and J_{CP}, predicted on the basis of the current data on the neutrino mixing parameters for each of the symmetry forms of $\tilde{U}_\nu$ considered. We recall that in the standard parametrisation of the PMNS matrix, the J_{CP} factor reads (see, e.g., [1]):

$$J_{CP} = \text{Im}\left\{U_{e1}^* U_{\mu3}^* U_{e3} U_{\mu1}\right\} = \frac{1}{8}\sin\delta\sin 2\theta_{13}\sin 2\theta_{23}\sin 2\theta_{12}\cos\theta_{13}. \tag{47}$$

We construct χ^2 for the schemes considered — TBM, BM (LC), GRA, GRB and HG — as described in Appendix B. We will focus on the general case of non-vanishing θ_{23}^e in order to allow for possible sizeable deviations of θ_{23} from the symmetry value $\pi/4$.

In the five panels in Fig. 11 we show $N_\sigma \equiv \sqrt{\chi^2}$ as a function of δ for the five symmetry forms of $\tilde{U}_\nu$ we have studied. The dashed lines correspond to the results of the global fit [11]. The solid lines represent the results we obtain by minimising the value of χ^2 in $\sin^2\theta_{13}$ and $\sin^2\theta_{23}$ (or, equivalently, in $\sin^2\theta_{12}^e$ and $\sin^2\hat{\theta}_{23}$) for a fixed value of δ.[9]

The blue (red) lines correspond to NO (IO) neutrino mass spectrum. The value of χ^2 at the minimum, $\chi^2_{\min}$, which determines the best fit value of δ predicted for each symmetry form of $\tilde{U}_\nu$, allows us to make conclusions about the compatibility of a given symmetry form of $\tilde{U}_\nu$ with the current global neutrino oscillation data.

It follows from the results shown in Fig. 11 that the BM (LC) symmetry form is disfavoured by the data at approximately 1.8σ, all the other symmetry forms considered being compatible with the data. We note that for the TBM, GRA, GRB and HG symmetry forms, a value of δ in the vicinity of $3\pi/2$ is preferred statistically. For the TBM symmetry form this result was first obtained in [13] while for the GRA, GRB and HG symmetry forms it was first found in [14]. In contrast, in the case of the BM (LC) form the best fit value is very close to π [13, 14]. The somewhat larger value of χ^2 at the second local minimum in the vicinity of $\pi/2$ in the TBM, GRA, GRB and HG cases, is a consequence of the fact that the best fit value of δ obtained in the global analysis of the current neutrino oscillation data is close to $3\pi/2$ and that the value of $\delta = \pi/2$ is statistically disfavoured (approximately at 2.5σ). In the absence of any information on δ, the two minima would have exactly the same value of χ^2, because they correspond to the same value of $\cos\delta$. In the schemes considered, as we have discussed, $\cos\delta$ is determined by the values of θ_{12}, θ_{13} and θ_{23}. The degeneracy in the sign of $\sin\delta$ can only be solved by an experimental input on δ. In Table 9 we give the best fit values of δ and the

---

[9] We note that in the scheme considered by us, fixing the value of δ implies that one of the three neutrino mixing angles is expressed in terms of the other two. We choose for convenience this angle to be θ_{12}.
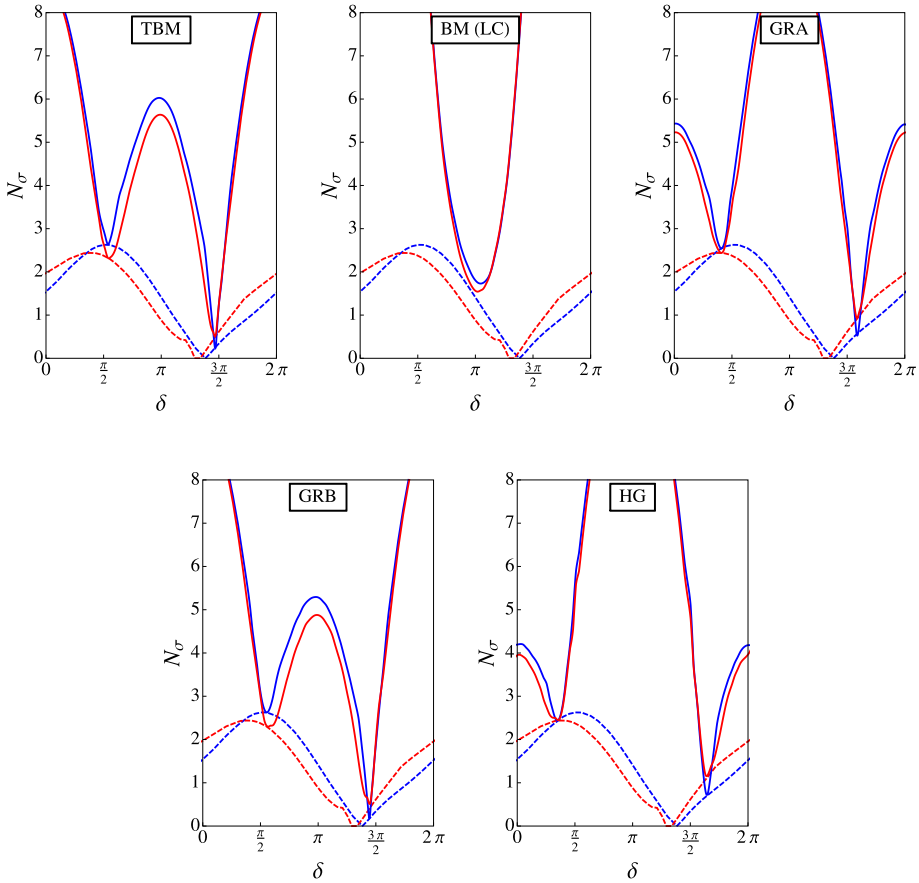
Fig. 11. $N_\sigma \equiv \sqrt{\chi^2}$ as a function of δ. The dashed lines represent the results of the global fit [11], while the solid lines represent the results we obtain for the TBM, BM (LC), GRA (upper left, central, right panels), GRB and HG (lower left and right panels) symmetry forms of $\tilde{U}_\nu$. The blue (red) lines are for NO (IO) neutrino mass spectrum (see text for further details). (For interpretation of the references to colour in this figure legend, the reader is referred to the web version of this article.)

corresponding 3σ ranges for the TBM, BM (LC), GRA, GRB and HG forms of $\tilde{U}_\nu$, found by fixing $\sqrt{\chi^2 - \chi^2_{\min}} = 3$.

In Fig. 12 we show the likelihood function versus $\cos\delta$ for NO neutrino mass spectrum. The results shown are obtained by marginalising over all the other relevant parameters of the scheme considered (see Appendix B for details). The dependence of the likelihood function on $\cos\delta$ in the case of IO neutrino mass spectrum differs little from that shown in Fig. 12. Given the global fit results, the likelihood function, i.e.,

$$L(\cos\delta) \propto \exp\left(-\frac{\chi^2(\cos\delta)}{2}\right), \tag{48}$$

represents the most probable value of $\cos\delta$ for each of the considered symmetry forms of $\tilde{U}_\nu$. The $n\sigma$ confidence level region corresponds to the interval of values of $\cos\delta$ in which $L(\cos\delta) \geq L(\chi^2 = \chi^2_{\min}) \cdot L(\chi^2 = n^2)$.

Table 9

Best fit values of J_{CP}, δ and $\cos\delta$ and corresponding 3σ ranges (found fixing $\sqrt{\chi^2 - \chi^2_{min}} = 3$) in our setup using the data from [11].

Symmetry form		Best fit	3σ range
TBM	J_{CP} (NO)	−0.034	−0.038 ÷ −0.028 ⊕ 0.031 ÷ 0.036
	J_{CP} (IO)	−0.034	−0.039 ÷ −0.025 ⊕ 0.029 ÷ 0.037
	δ/π (NO)	1.48	0.49 ÷ 0.58 ⊕ 1.34 ÷ 1.57
	δ/π (IO)	1.48	0.47 ÷ 0.65 ⊕ 1.30 ÷ 1.57
	$\cos\delta$ (NO)	−0.07	−0.47 ÷ 0.21
	$\cos\delta$ (IO)	−0.07	−0.60 ÷ 0.23
BM (LC)	J_{CP} (NO)	−0.005	−0.026 ÷ 0.021
	J_{CP} (IO)	−0.002	−0.025 ÷ 0.023
	δ/π (NO)	1.04	0.80 ÷ 1.24
	δ/π (IO)	1.02	0.79 ÷ 1.23
	$\cos\delta$ (NO)	−0.99	−1.00 ÷ −0.72
	$\cos\delta$ (IO)	−1.00	−1.00 ÷ −0.72
GRA	J_{CP} (NO)	−0.033	−0.037 ÷ −0.027 ⊕ 0.030 ÷ 0.035
	J_{CP} (IO)	−0.033	−0.037 ÷ −0.025 ⊕ 0.028 ÷ 0.036
	δ/π (NO)	1.58	0.35 ÷ 0.46 ⊕ 1.50 ÷ 1.70
	δ/π (IO)	1.58	0.31 ÷ 0.48 ⊕ 1.47 ÷ 1.74
	$\cos\delta$ (NO)	0.25	−0.08 ÷ 0.69
	$\cos\delta$ (IO)	0.25	−0.08 ÷ 0.69
GRB	J_{CP} (NO)	−0.034	−0.039 ÷ −0.026 ⊕ 0.031 ÷ 0.036
	J_{CP} (IO)	−0.033	−0.039 ÷ −0.022 ⊕ 0.026 ÷ 0.037
	δ/π (NO)	1.45	0.51 ÷ 0.61 ⊕ 1.31 ÷ 1.54
	δ/π (IO)	1.45	0.50 ÷ 0.70 ⊕ 1.25 ÷ 1.54
	$\cos\delta$ (NO)	−0.15	−0.57 ÷ 0.13
	$\cos\delta$ (IO)	−0.15	−0.70 ÷ 0.13
HG	J_{CP} (NO)	−0.031	−0.035 ÷ −0.020 ⊕ 0.026 ÷ 0.034
	J_{CP} (IO)	−0.031	−0.036 ÷ −0.015 ⊕ 0.019 ÷ 0.034
	δ/π (NO)	1.66	0.27 ÷ 0.41 ⊕ 1.55 ÷ 1.80
	δ/π (IO)	1.63	0.19 ÷ 0.42 ⊕ 1.55 ÷ 1.86
	$\cos\delta$ (NO)	0.47	0.16 ÷ 0.80
	$\cos\delta$ (IO)	0.40	0.16 ÷ 0.80

As can be observed from Fig. 12, a rather precise measurement of $\cos\delta$ would allow one to distinguish between the different symmetry forms of $\tilde{U}_\nu$ considered by us. For the TBM and GRB forms there is a significant overlap of the corresponding likelihood functions. The same observation is valid for the GRA and HG forms. However, the overlap of the likelihood functions of these two groups of symmetry forms occurs only at 3σ level in a very small interval of values of $\cos\delta$, as can also be seen from Table 9. This implies that in order to distinguish between TBM/GRB, GRA/HG and BM symmetry forms a not very demanding measurement (in terms of accuracy) of $\cos\delta$ might be sufficient. The value of the non-normalised likelihood function at the maximum in Fig. 12 is equal to $\exp(-\chi^2_{min}/2)$, which allows us to make conclusions about the compatibility of the symmetry schemes with the current global data, as has already been pointed out.

In the left panel of Fig. 13 we present the likelihood function versus $\cos\delta$ within the Gaussian approximation (see Appendix B for details), using the current best fit values of the mixing angles for NO neutrino mass spectrum in Eqs. (3)–(5) and the prospective 1σ uncertainties in
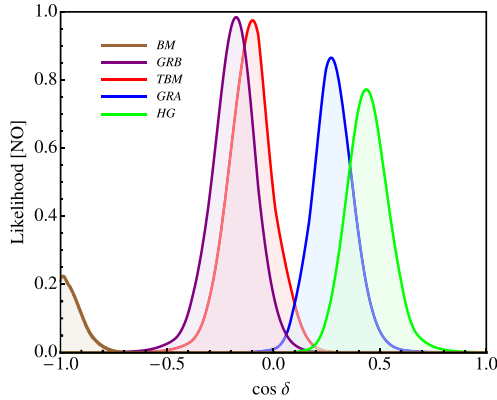
Fig. 12. The likelihood function versus $\cos\delta$ for NO neutrino mass spectrum after marginalising over $\sin^2\theta_{13}$ and $\sin^2\theta_{23}$ for the TBM, BM (LC), GRA, GRB and HG symmetry forms of the mixing matrix $\tilde{U}_\nu$ (see text for further details). (For interpretation of the references to colour in this figure legend, the reader is referred to the web version of this article.)
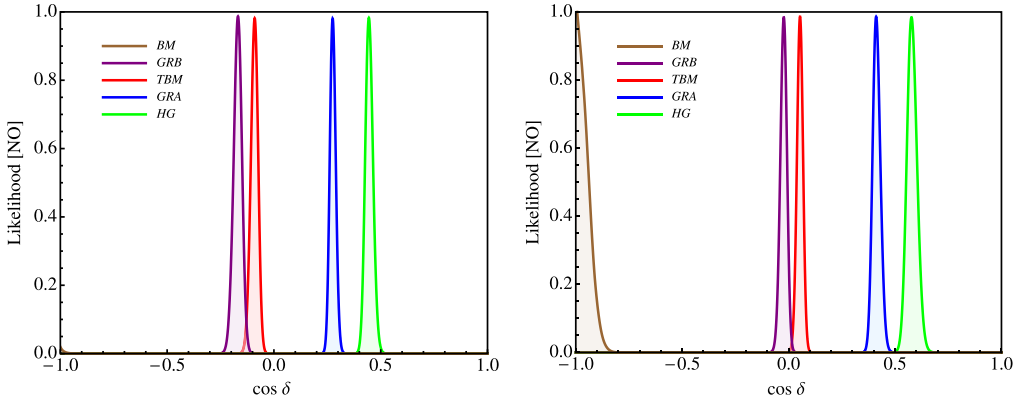

Fig. 13. The same as in Fig. 12, but using the prospective 1σ uncertainties in the determination of the neutrino mixing angles within the Gaussian approximation (see text for further details). In the left (right) panel $\sin^2\theta_{12} = 0.308 \, (0.332)$, the other mixing angles being fixed to their NO best fit values.

the determination of $\sin^2\theta_{12}$ (0.7% from JUNO [48]), $\sin^2\theta_{13}$ (almost 3% derived from an expected error on $\sin^2 2\theta_{13}$ of 3% from Daya Bay, see A. de Gouvea et al. in [2]) and $\sin^2\theta_{23}$ (5%[10] derived from the potential sensitivity of NOvA and T2K on $\sin^2 2\theta_{23}$ of 2%, see A. de Gouvea et al. in [2]). The BM case is very sensitive to the best fit values of $\sin^2\theta_{12}$ and $\sin^2\theta_{23}$ and is disfavoured at more than 2σ for the current best fit values quoted in Eqs. (3)–(5). This case might turn out to be compatible with the data for larger (smaller) measured values of $\sin^2\theta_{12}$ ($\sin^2\theta_{23}$), as can be seen from the right panel of Fig. 13, which was obtained for $\sin^2\theta_{12} = 0.332$. With the increase of the value of $\sin^2\theta_{23}$ the BM form becomes increasingly disfavoured, while the TBM/GRB (GRA/HG) predictions for $\cos\delta$ are shifted somewhat — approximately by 0.1 — to the left (right) with respect to those shown in the left panel of Fig. 13. This shift is illustrated in Fig. 14, which is obtained for $\sin^2\theta_{23} = 0.579$, more precisely, for the best fit values found in

---

[10] This sensitivity can be achieved in future neutrino facilities [49].
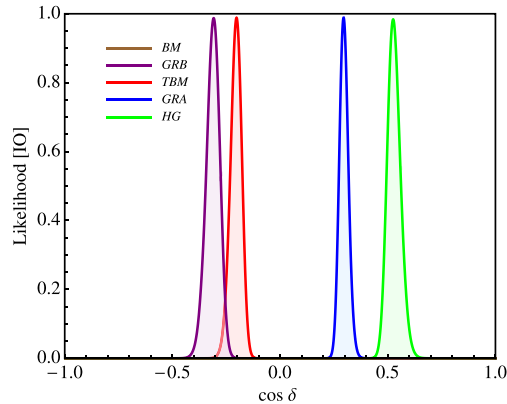
Fig. 14. The same as in Fig. 13, but using the IO best fit values taken from [12].

[12] and corresponding to IO neutrino mass spectrum. The measurement of $\sin^2\theta_{12}$, $\sin^2\theta_{13}$ and $\sin^2\theta_{23}$ with the quoted precision will open up the possibility to distinguish between the BM, TBM/GRB, GRA and HG forms of $\tilde{U}_\nu$. Distinguishing between the TBM and GRB forms would require relatively high precision measurement of $\cos\delta$.

We have performed also a statistical analysis in order to derive predictions for J_{CP}. In Fig. 15 we present $N_\sigma \equiv \sqrt{\chi^2}$ as a function of J_{CP} for NO and IO neutrino mass spectra. Similarly to the case of δ, we minimise the value of χ^2 for a fixed value of J_{CP} by varying $\sin^2\theta_{13}$ and $\sin^2\theta_{23}$ (or, equivalently, $\sin^2\theta_{12}^e$ and $\sin^2\hat{\theta}_{23}$). The best fit value of J_{CP} and the corresponding 3σ range for each of the considered symmetry forms of $\tilde{U}_\nu$ are summarised in Table 9. As Fig. 15 shows, the CP-conserving value of $J_{CP} = 0$ is excluded in the cases of the TBM, GRA, GRB and HG neutrino mixing symmetry forms, respectively, at approximately 5σ, 4σ, 4σ and 3σ confidence levels with respect to the confidence level of the corresponding best fit values.[11]

These results correspond to those we have obtained for δ, more specifically to the confidence levels at which the CP-conserving values of $\delta = 0$, π, 2π, are excluded (see Fig. 11).

In contrast, for the BM (LC) symmetry form, the CP-conserving value of δ, namely, $\delta \cong \pi$, is preferred and therefore the CP-violating effects in neutrino oscillations are predicted to be suppressed. At the best fit point we obtain a value of $J_{CP} = -0.005\,(-0.002)$ for NO (IO) neutrino mass spectrum, which corresponds to the best fit value of $\delta/\pi = 1.04\,(1.02)$. The allowed range of the J_{CP} factor in the BM (LC) includes the CP-conserving value $J_{CP} = 0$ at practically any confidence level. As can be seen from Table 9, the 3σ allowed intervals of values of δ and J_{CP} are rather narrow for all the symmetry forms considered, except for the BM (LC) form.

Finally, for completeness, we present in Appendix C also results of a statistical analysis of the predictions for the values of $\sin^2\theta_{23}$ for the TBM, BM (LC), GRA, GRB and HG neutrino mixing symmetry forms considered. We recall that of the three neutrino mixing parameters, $\sin^2\theta_{12}$, $\sin^2\theta_{13}$ and $\sin^2\theta_{23}$, $\sin^2\theta_{23}$ is determined in the global analyses of the neutrino oscillation data with the largest uncertainty.

---

[11] The confidence levels under discussion differ in the cases of NO and IO neutrino mass spectra, but as Fig. 15 indicates, in the cases considered these differences are rather small and we have not given them.
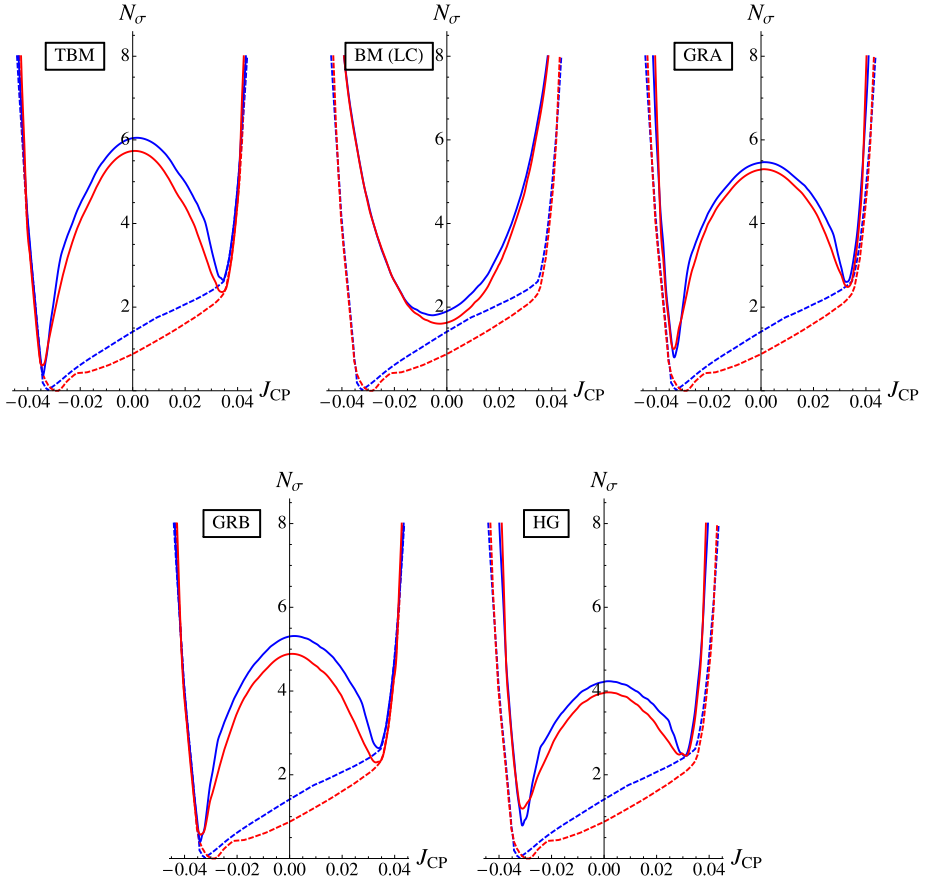
Fig. 15. $N_\sigma \equiv \sqrt{\chi^2}$ as a function of J_{CP}. The dashed lines represent the results of the global fit [11], while the solid lines represent the results we obtain for the TBM, BM (LC), GRA (upper left, central, right panels), GRB and HG (lower left and right panels) neutrino mixing symmetry forms. The blue (red) lines are for NO (IO) neutrino mass spectrum (see text for further details). (For interpretation of the references to colour in this figure legend, the reader is referred to the web version of this article.)

6. Summary and conclusions

Using the fact that the neutrino mixing matrix $U = U_e^\dagger U_\nu$, where U_e and U_ν result from the diagonalisation of the charged lepton and neutrino mass matrices, we have analysed the sum rules which the Dirac phase δ present in U satisfies when U_ν has a form dictated by, or associated with, discrete symmetries and U_e has a "minimal" form (in terms of angles and phases it contains) that can provide the requisite corrections to U_ν, so that the reactor, atmospheric and solar neutrino mixing angles θ_{13}, θ_{23} and θ_{12} have values compatible with the current data.

We have considered the following symmetry forms of U_ν: i) tri-bimaximal (TBM), ii) bi-maximal (BM) (or corresponding to the conservation of the lepton charge $L' = L_e - L_\mu - L_\tau$ (LC)), iii) golden ratio type A (GRA), iv) golden ratio type B (GRB), and v) hexagonal (HG). For all these symmetry forms U_ν can be written as $U_\nu = \Psi_1 \tilde{U}_\nu Q_0 = \Psi_1 R_{23}(\theta_{23}^\nu) R_{12}(\theta_{12}^\nu) Q_0$, where $R_{23}(\theta_{23}^\nu)$ and $R_{12}(\theta_{12}^\nu)$ are orthogonal matrices describing rotations in the 2-3 and 1-2

planes, respectively, and Ψ_1 and Q_0 are diagonal phase matrices each containing two phases. The phases in the matrix Q_0 give contribution to the Majorana phases in the PMNS matrix. The symmetry forms of $\tilde{U}_\nu$ of interest, TBM, BM (LC), GRA, GRB and HG, are characterised by the same value of the angle $\theta_{23}^\nu = -\pi/4$, but correspond to different fixed values of the angle θ_{12}^ν and thus of $\sin^2 \theta_{12}^\nu$, namely, to i) $\sin^2 \theta_{12}^\nu = 1/3$ (TBM), ii) $\sin^2 \theta_{12}^\nu = 1/2$ (BM (LC)), iii) $\sin^2 \theta_{12}^\nu = (2+r)^{-1} \cong 0.276$ (GRA), r being the golden ratio, $r = (1 + \sqrt{5})/2$, iv) $\sin^2 \theta_{12}^\nu = (3 - r)/4 \cong 0.345$ (GRB), and v) $\sin^2 \theta_{12}^\nu = 1/4$ (HG).

The minimal form of U_e of interest that can provide the requisite corrections to U_ν, so that the neutrino mixing angles θ_{13}, θ_{23} and θ_{12} have values compatible with the current data, including a possible sizeable deviation of θ_{23} from $\pi/4$, includes a product of two orthogonal matrices describing rotations in the 2-3 and 1-2 planes [13], $R_{23}(\theta_{23}^e)$ and $R_{12}(\theta_{12}^e)$, θ_{23}^e and θ_{12}^e being two (real) angles. This leads to the parametrisation of the PMNS matrix U given in Eq. (11), which can be recast in the form [13]: $U = R_{12}(\theta_{12}^e) \Phi(\phi) R_{23}(\hat{\theta}_{23}) R_{12}(\theta_{12}^\nu) \hat{Q}$, where $\Phi = \mathrm{diag}\left(1, e^{i\phi}, 1\right)$, ϕ being a CP violation phase, $\hat{\theta}_{23}$ is a function of θ_{23}^e (see Eq. (14)), and $\hat{Q}$ is a diagonal phase matrix. The phases in $\hat{Q}$ give contributions to the Majorana phases in the PMNS matrix. The angle $\hat{\theta}_{23}$, however, can be expressed in terms of the angles θ_{23} and θ_{13} of the PMNS matrix (Eq. (20)) and the value of $\hat{\theta}_{23}$ is fixed by the values of θ_{23} and θ_{13}.

In this scheme the four observables θ_{12}, θ_{23}, θ_{13} and the Dirac phase δ in the PMNS matrix are functions of three parameters θ_{12}^e, $\hat{\theta}_{23}$ and ϕ. As a consequence, the Dirac phase δ can be expressed as a function of the three PMNS angles θ_{12}, θ_{23} and θ_{13}, leading to a new "sum rule" relating δ and θ_{12}, θ_{23} and θ_{13}. This sum rule is exact within the scheme considered. Its explicit form depends on the symmetry form of the matrix $\tilde{U}_\nu$, i.e., on the value of the angle θ_{12}^ν. For arbitrary fixed value of θ_{12}^ν the sum rule of interest is given in Eq. (22) (or the equivalent Eq. (23)) [14]. A similar exact sum rule can be derived for the phase ϕ (Eq. (24)) [14].

A parametrisation of the PMNS matrix, similar to that given in Eq. (11), has been effectively employed in Ref. [15]. Treating $\sin \theta_{12}^e$ and $\sin \theta_{23}^e$ as small parameters, $|\sin \theta_{12}^e| \ll 1$, $|\sin \theta_{23}^e| \ll 1$, and neglecting terms of order of, or smaller than, $O((\theta_{12}^e)^2)$, $O((\theta_{23}^e)^2)$ and $O(\theta_{12}^e \theta_{23}^e)$, the following "leading order" sum rule was obtained in [15]: $\theta_{12} \cong \theta_{12}^\nu + \theta_{13} \cos \delta$. This sum rule, in the approximation used to obtain it, is equivalent to the sum rule $\sin \theta_{12} \cong \sin \theta_{12}^\nu + \cos \theta_{12}^\nu \sin \theta_{13} \cos \delta$, which was shown in Ref. [14] to be the leading order approximation of the exact sum rule given in Eq. (22) (or the equivalent Eq. (23)). In the present article we have investigated the predictions for $\cos \delta$ in the cases of TBM, BM (LC), GRA, GRB and HG symmetry forms of the matrix $\tilde{U}_\nu$ using the exact and the leading order sum rules for $\cos \delta$ discussed above and given in Eqs. (23) and (30). It was shown in [14], in particular, using the best fit values of the neutrino mixing parameters $\sin^2 \theta_{12}$, $\sin^2 \theta_{23}$ and $\sin^2 \theta_{13}$ and the exact sum rule results for $\cos \delta$ derived for the TBM, GRA, GRB and HG forms of $\tilde{U}_\nu$, that the leading order sum rule provides largely imprecise predictions for $\cos \delta$. Here we have performed a thorough study of the exact and leading order sum rule predictions for $\cos \delta$ in the TBM, BM (LC), GRA, GRB and HG cases taking into account the uncertainties in the measured values of $\sin^2 \theta_{12}$, $\sin^2 \theta_{23}$ and $\sin^2 \theta_{13}$. This allowed us, in particular, to assess the accuracy of the predictions for $\cos \delta$ based on the leading order sum rules and its dependence on the values of the indicated neutrino mixing parameters when the latter are varied in their respective 3σ experimentally allowed ranges. In contrast to the leading order sum rule, the exact sum rule for $\cos \delta$ depends not only on θ_{12} and θ_{13}, but also on θ_{23}, and we have investigated this dependence as well.

In the present study we have analysed both the cases of $\theta_{23}^e = 0$, in which $\sin^2 \theta_{23} \cong 0.5(1 - \sin^2 \theta_{13})$, and of arbitrary θ_{23}^e. In the second case θ_{23} can deviate significantly from $\pi/4$.

We confirm the result found in [14] that the exact sum rule predictions for $\cos \delta$ vary significantly with the symmetry form of $\tilde{U}_\nu$. This result implies that the measurement of $\cos \delta$ can allow us to distinguish between the different symmetry forms of $\tilde{U}_\nu$ [14] provided $\sin^2 \theta_{12}$, $\sin^2 \theta_{13}$ and $\sin^2 \theta_{23}$ are known with a sufficiently good precision. Even determining the sign of $\cos \delta$ will be sufficient to eliminate some of the possible symmetry forms of $\tilde{U}_\nu$.

We find also that the exact sum rule predictions for $\cos \delta$ exhibit strong dependence on the value of $\sin^2 \theta_{12}$ when the latter is varied in its 3σ experimentally allowed range (0.259–0.359) (Tables 1–6). The predictions for $\cos \delta$ change significantly not only in magnitude, but in the cases of TBM, GRA and GRB forms of $\tilde{U}_\nu$ also the sign of $\cos \delta$ can change. These significant changes take place both for $\theta^e_{23} = 0$ and $\theta^e_{23} \neq 0$.

We have investigated the dependence of the exact sum rule predictions for $\cos \delta$ in the cases of the symmetry forms of $\tilde{U}_\nu$ considered on the value of $\sin^2 \theta_{23}$ varying the latter in the respective 3σ allowed interval $0.374 \leq \sin^2 \theta_{23} \leq 0.626$ (Figs. 9 and 10, and Tables 7 and 8). The results we get for $\sin^2 \theta_{23} = 0.374$ and $\sin^2 \theta_{23} = 0.437$, setting $\sin^2 \theta_{12}$ and $\sin^2 \theta_{13}$ to their best fit values, do not differ significantly. However, the differences between the predictions for $\cos \delta$ obtained for $\sin^2 \theta_{23} = 0.437$ and for $\sin^2 \theta_{23} = 0.626$ are relatively large (they differ by the factors of 2.05, 1.25, 1.77 and 1.32 in the TBM, GRA, GRB and HG cases, respectively).

In all cases considered, having the exact sum rule results for $\cos \delta$, we could investigate the precision of the leading order sum rule predictions for $\cos \delta$. We found that the leading order sum rule predictions for $\cos \delta$ are, in general, imprecise and in many cases are largely incorrect, the only exception being the case of the BM (LC) form of $\tilde{U}_\nu$ [14].

We have performed a similar analysis of the predictions for the cosine of the phase ϕ. The phase ϕ is related to, but does not coincide with, the Dirac phase δ. The parameter $\cos \phi$ obeys a leading order sum rule which is almost identical to the leading order sum rule satisfied by $\cos \delta$. This leads to the confusing identification of ϕ with δ: the exact sum rules satisfied by $\cos \phi$ and $\cos \delta$ differ significantly. Correspondingly, the predicted values of $\cos \phi$ and $\cos \delta$ in the cases of the TBM, GRA, GRB and HG symmetry forms of $\tilde{U}_\nu$ considered by us also differ significantly (see Figs. 1–10 and Tables 1–8). This conclusion is not valid for the BM (LC) form: for this form the exact sum rule predictions for $\cos \phi$ and $\cos \delta$ are rather similar. The phase ϕ appears in a large class of models of neutrino mixing and neutrino mass generation and serves as a "source" for the Dirac phase δ in these models.

Finally, we have performed a statistical analysis of the predictions for δ, $\cos \delta$ and the rephasing invariant J_{CP} which controls the magnitude of CPV effects in neutrino oscillations [47], in the cases of the TBM, BM (LC), GRA, GRB and HG symmetry forms of the matrix $\tilde{U}_\nu$ considered. In this analysis we have used as input the latest results on $\sin^2 \theta_{12}$, $\sin^2 \theta_{13}$, $\sin^2 \theta_{23}$ and δ, obtained in the global analysis of the neutrino oscillation data performed in [11]. Our goal was to derive the allowed ranges for δ, $\cos \delta$ and J_{CP}, predicted on the basis of the current data on the neutrino mixing parameters for each of the symmetry forms of $\tilde{U}_\nu$ considered. The results of this analysis are shown in Figs. 11, 12 and 15, and are summarised in Table 9, in which we give the predicted best fit values and 3σ ranges of J_{CP}, δ and $\cos \delta$ for each of the symmetry forms of $\tilde{U}_\nu$ considered. We have shown, in particular, that the CP-conserving value of $J_{CP} = 0$ is excluded in the cases of the TBM, GRA, GRB and HG neutrino mixing symmetry forms, respectively, at approximately 5σ, 4σ, 4σ and 3σ confidence levels with respect to the confidence level of the corresponding best fit values (Fig. 15). These results reflect the predictions we have obtained for δ, more specifically, the confidence levels at which the CP-conserving values of $\delta = 0$, π, 2π, are excluded in the discussed cases (see Fig. 11). We have found also that the 3σ allowed intervals of values of δ and J_{CP} are rather narrow for all the symmetry forms con-

sidered, except for the BM (LC) form (Table 9). More specifically, for the TBM, GRA, GRB and HG symmetry forms we have obtained at 3σ: $0.020 \leq |J_{CP}| \leq 0.039$. For the best fit values of J_{CP} we have found, respectively: $J_{CP} = (-0.034), (-0.033), (-0.034)$, and (-0.031). Our results indicate that distinguishing between the TBM, GRA, GRB and HG symmetry forms of the neutrino mixing would require extremely high precision measurement of the J_{CP} factor.

Using the likelihood method, we have derived also the ranges of the predicted values of $\cos\delta$ for the different forms of $\tilde{U}_\nu$ considered, using the prospective 1σ uncertainties in the determination of $\sin^2\theta_{12}$, $\sin^2\theta_{13}$ and $\sin^2\theta_{23}$ respectively in JUNO, Daya Bay and accelerator and atmospheric neutrino experiments (Fig. 13). In this analysis the current best fit values of $\sin^2\theta_{12}$, $\sin^2\theta_{13}$ and $\sin^2\theta_{23}$ have been utilised (left panel of Fig. 13). The results thus obtained show that i) the measurement of the sign of $\cos\delta$ will allow to distinguish between the TBM/GRB, BM and GRA/HG forms of $\tilde{U}_\nu$, ii) for a best fit value of $\cos\delta = -1\,(-0.1)$ distinguishing at 3σ between the BM (TBM/GRB) and the other forms of $\tilde{U}_\nu$ would be possible if $\cos\delta$ is measured with 1σ uncertainty of $0.3\,(0.1)$.

The predictions for δ, $\cos\delta$ and J_{CP} in the case of the BM (LC) symmetry form of $\tilde{U}_\nu$, as the results of the statistical analysis performed by us showed, differ significantly from those found for the TBM, GRA, GRB and HG forms: the best fit value of $\delta \cong \pi$, and, correspondingly, of $J_{CP} \cong 0$. For the 3σ range of J_{CP} we have obtained in the case of NO (IO) neutrino mass spectrum: $-0.026\,(-0.025) \leq J_{CP} \leq 0.021\,(0.023)$, i.e., it includes a sub-interval of values centred on zero, which does not overlap with the 3σ allowed intervals of values of J_{CP} in the TBM, GRA, GRB and HG cases.

The results obtained in the present study, in particular, reinforce the conclusion reached in Ref. [14] that the experimental measurement of the cosine of the Dirac phase δ of the PMNS neutrino mixing matrix can provide unique information about the possible discrete symmetry origin of the observed pattern of neutrino mixing.

Acknowledgements

Appendix A. Relations between phases in two parametrisations

In this section we present the relations between the phases of the two different parametrisations of the PMNS matrix employed in [15] and [14]. In the parametrisation used in [15] the PMNS matrix after setting $\theta_{13}^e = \theta_{13}^\nu = 0$ reads:

$$U_{\text{PMNS}} = U_{12}^{e_L\,\dagger}\, U_{23}^{e_L\,\dagger}\, U_{23}^{\nu_L}\, U_{12}^{\nu_L}, \tag{49}$$

where the subscripts 12 and 23 stand for the rotation plane, e.g., the matrix $U_{12}^{e_L}$ being defined as

$$U_{12}^{e_L} = \begin{pmatrix} \cos\theta_{12}^e & \sin\theta_{12}^e\, e^{-i\delta_{12}^e} & 0 \\ -\sin\theta_{12}^e\, e^{i\delta_{12}^e} & \cos\theta_{12}^e & 0 \\ 0 & 0 & 1 \end{pmatrix}, \tag{50}$$

and the others analogously. We can factorise the phases in the charged lepton and the neutrino sectors in the following way:

$$
U_{12}^{eL\dagger} U_{23}^{eL\dagger} = \begin{pmatrix} 1 & 0 & 0 \\ 0 & e^{i(\delta_{12}^e+\pi)} & 0 \\ 0 & 0 & e^{i(\delta_{12}^e+\delta_{23}^e)} \end{pmatrix} \begin{pmatrix} \cos\theta_{12}^e & \sin\theta_{12}^e & 0 \\ -\sin\theta_{12}^e & \cos\theta_{12}^e & 0 \\ 0 & 0 & 1 \end{pmatrix}
$$

$$
\times \begin{pmatrix} 1 & 0 & 0 \\ 0 & \cos\theta_{23}^e & \sin\theta_{23}^e \\ 0 & -\sin\theta_{23}^e & \cos\theta_{23}^e \end{pmatrix} \begin{pmatrix} 1 & 0 & 0 \\ 0 & e^{-i(\delta_{12}^e+\pi)} & 0 \\ 0 & 0 & e^{-i(\delta_{12}^e+\delta_{23}^e)} \end{pmatrix}, \tag{51}
$$

$$
U_{23}^{\nu L} U_{12}^{\nu L} = \begin{pmatrix} 1 & 0 & 0 \\ 0 & e^{i\delta_{12}^\nu} & 0 \\ 0 & 0 & e^{i(\delta_{23}^\nu+\delta_{12}^\nu)} \end{pmatrix} \begin{pmatrix} 1 & 0 & 0 \\ 0 & \cos\theta_{23}^\nu & \sin\theta_{23}^\nu \\ 0 & -\sin\theta_{23}^\nu & \cos\theta_{23}^\nu \end{pmatrix}
$$

$$
\times \begin{pmatrix} \cos\theta_{12}^\nu & \sin\theta_{12}^\nu & 0 \\ -\sin\theta_{12}^\nu & \cos\theta_{12}^\nu & 0 \\ 0 & 0 & 1 \end{pmatrix} \begin{pmatrix} 1 & 0 & 0 \\ 0 & e^{-i\delta_{12}^\nu} & 0 \\ 0 & 0 & e^{-i(\delta_{23}^\nu+\delta_{12}^\nu)} \end{pmatrix}. \tag{52}
$$

Combining Eqs. (51) and (52) and comparing with the parametrisation of the PMNS matrix employed in [14] and given in Eqs. (11) and (12), we find the following relations:

$$
\psi = \delta_{12}^e - \delta_{12}^\nu + \pi, \quad \omega = \delta_{23}^e + \delta_{12}^e - \delta_{23}^\nu - \delta_{12}^\nu, \tag{53}
$$

$$
\xi_{21} = -2\delta_{12}^\nu, \quad \xi_{31} = -2(\delta_{12}^\nu + \delta_{23}^\nu). \tag{54}
$$

Appendix B. Statistical details

In order to perform a statistical analysis of the models considered we construct the χ^2 function in the following way:

$$
\chi^2(\sin^2\theta_{12}, \sin^2\theta_{13}, \sin^2\theta_{23}, \delta)
$$
$$
= \chi_1^2(\sin^2\theta_{12}) + \chi_2^2(\sin^2\theta_{13}) + \chi_3^2(\sin^2\theta_{23}) + \chi_4^2(\delta), \tag{55}
$$

in which we have neglected the correlations among the oscillation parameters, since the functions χ_i^2 have been extracted from the 1-dimensional projections in [11]. In order to quantify the accuracy of our approximation we show in Fig. 16 the confidence regions at 1σ, 2σ and 3σ for 1 degree of freedom in the planes $(\sin^2\theta_{23}, \delta)$, $(\sin^2\theta_{13}, \delta)$ and $(\sin^2\theta_{23}, \sin^2\theta_{13})$ in blue (dashed lines), purple (solid lines) and light-purple (dash-dotted lines) for NO (IO) neutrino mass spectrum, respectively, obtained using Eq. (55). The parameters not shown in the plot have been marginalised. It should be noted that what is also used in the literature is the Gaussian approximation, in which χ^2 can be simplified using the best fit values and the 1σ uncertainties as follows:

$$
\chi_G^2 = \sum_i \frac{(x_i - \bar{x}_i)^2}{\sigma_{x_i}^2}. \tag{56}
$$

Here $x_i = \{\sin^2\theta_{12}, \sin^2\theta_{13}, \sin^2\theta_{23}, \delta\}$, $\bar{x}_i$ and σ_{x_i} being the best fit values and the 1σ uncertainties[12] taken from [11]. We present in Fig. 17 the results of a similar two-dimensional analysis

---

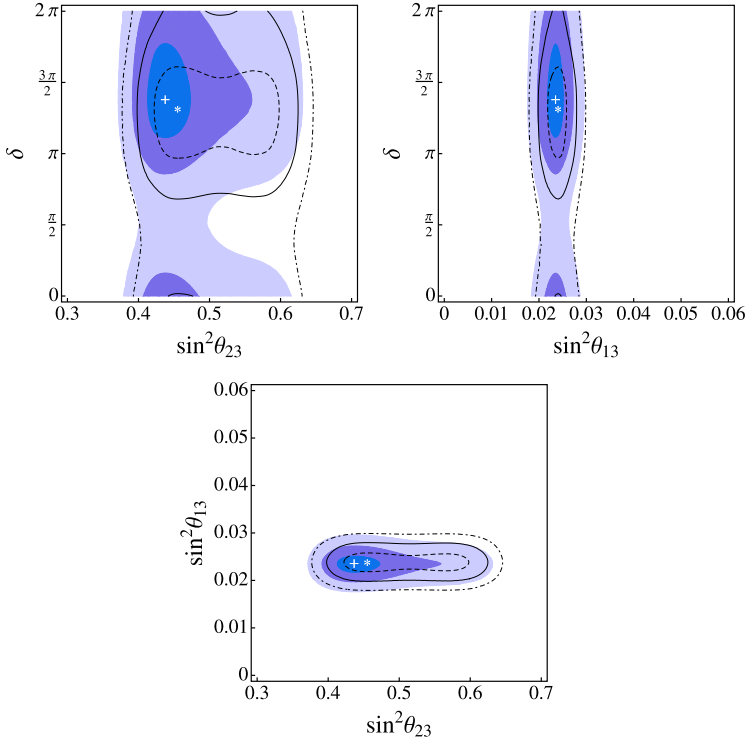[12] In the case of asymmetric errors we take the mean value of the two errors.

Fig. 16. Confidence regions at 1σ, 2σ and 3σ for 1 degree of freedom in the planes $(\sin^2\theta_{23}, \delta)$, $(\sin^2\theta_{13}, \delta)$ and $(\sin^2\theta_{23}, \sin^2\theta_{13})$ in the blue (dashed lines), purple (solid lines) and light-purple (dash-dotted lines) for NO (IO) neutrino mass spectrum, respectively, obtained using Eq. (55). The best fit points are indicated with a cross (NO) and an asterisk (IO). (For interpretation of the references to colour in this figure legend, the reader is referred to the web version of this article.)

for the confidence level regions in the planes shown in Fig. 16, but using the approximation for χ^2 given in Eq. (56). It follows from these figures that the Gaussian approximation does not allow to reproduce the confidence regions of [11] with sufficiently good accuracy. For this reason in our analysis we use the more accurate procedure defined through Eq. (55). In both the figures the best fit points are indicated with a cross and an asterisk for NO and IO spectra, respectively.

Each symmetry scheme considered in our analysis, which we label with an index m, depends on a set of parameters y_j^m, which are related to the standard oscillation parameters through expressions of the form $x_i = x_i^m(y_j^m)$. In order to produce the 1-dimensional figures we minimise

$$\chi^2\left(x_i^m(y_j^m)\right) = \sum_{i=1}^{4} \chi_i^2\left(x_i^m(y_j^m)\right) \tag{57}$$

for a fixed value of the corresponding observable α, i.e.,

$$\chi^2(\alpha) = \min\left[\chi^2\left(x_i^m(y_j^m)\right)\big|_{\alpha=\text{const}}\right], \tag{58}$$

with $\alpha = \{\delta, J_{\text{CP}}, \sin^2\theta_{23}\}$. The likelihood function for $\cos\delta$ has been computed by taking
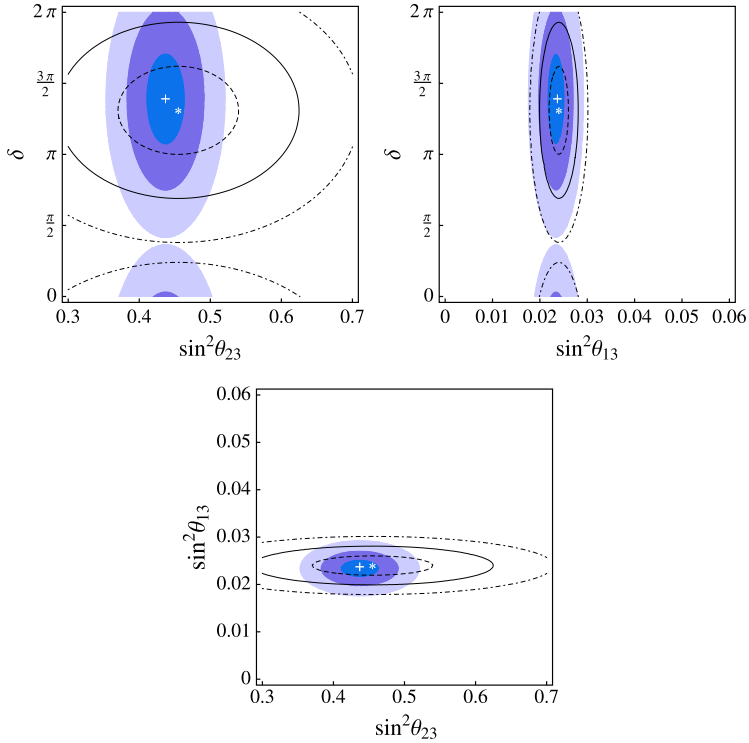
Fig. 17. The same as in Fig. 16, but using Eq. (56).

Table 10
Best fit values of $\sin^2\theta_{23}$ and corresponding 3σ ranges (found fixing $\sqrt{\chi^2 - \chi^2_{\min}} = 3$) in our setup using the data from [11].

Symmetry form		Best fit	3σ range
TBM	$\sin^2\theta_{23}$ (NO)	0.44	$0.37 \div 0.63$
	$\sin^2\theta_{23}$ (IO)	0.46	$0.38 \div 0.65$
BM (LC)	$\sin^2\theta_{23}$ (NO)	0.42	$0.37 \div 0.52$
	$\sin^2\theta_{23}$ (IO)	0.42	$0.37 \div 0.56$
GRA	$\sin^2\theta_{23}$ (NO)	0.44	$0.37 \div 0.63$
	$\sin^2\theta_{23}$ (IO)	0.46	$0.38 \div 0.65$
GRB	$\sin^2\theta_{23}$ (NO)	0.44	$0.37 \div 0.63$
	$\sin^2\theta_{23}$ (IO)	0.46	$0.38 \div 0.65$
HG	$\sin^2\theta_{23}$ (NO)	0.44	$0.37 \div 0.63$
	$\sin^2\theta_{23}$ (IO)	0.46	$0.38 \div 0.64$

$$L(\cos\delta) \propto \exp\left(-\frac{\chi^2(\cos\delta)}{2}\right),\tag{59}$$

which was used to produce the likelihood function for the different symmetry forms in Fig. 12. It is worth noticing that in the case of flat priors on the mixing parameters, the posterior proba-
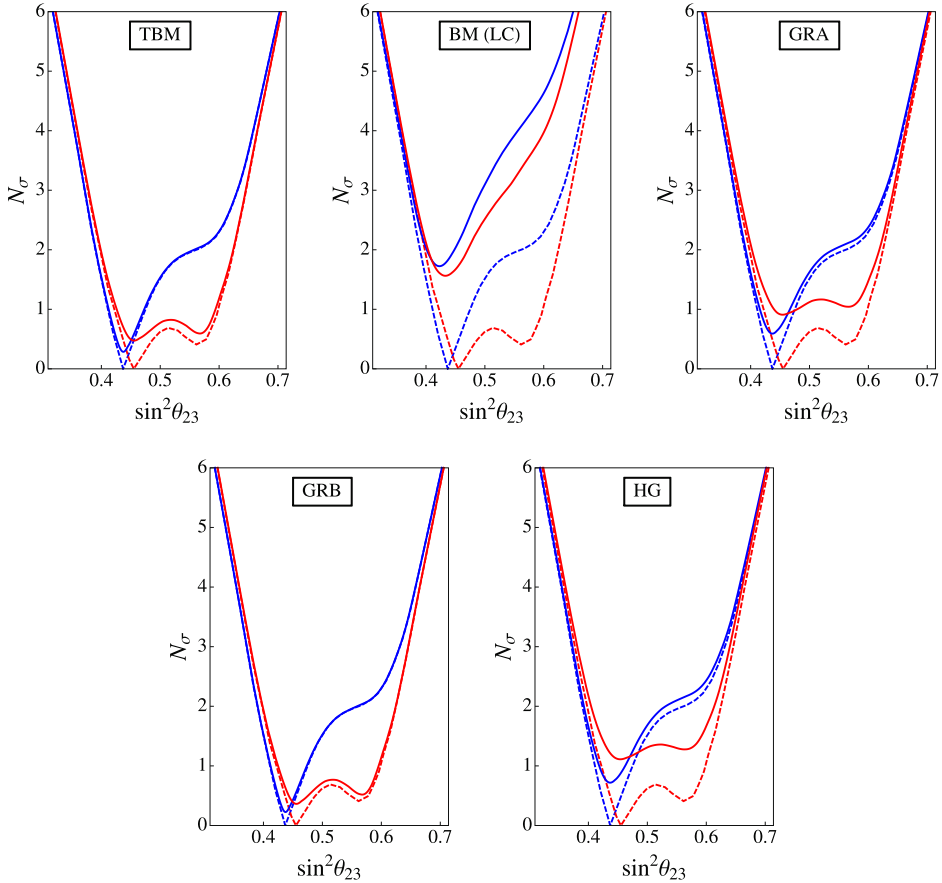
Fig. 18. $N_\sigma \equiv \sqrt{\chi^2}$ as a function of $\sin^2\theta_{23}$. The dashed lines represent the results of the global fit [11], while the solid ones represent the results we obtain for the TBM, BM (LC), GRA (upper left, central, right panels), GRB and HG (lower left and right panels) neutrino mixing symmetry forms. The blue (red) lines are for NO (IO) neutrino mass spectrum. (For interpretation of the references to colour in this figure legend, the reader is referred to the web version of this article.)

bility density function reduces to the likelihood function. Although we did not use the Gaussian approximation for obtaining Figs. 11, 12, 15 and 18, we employed it to obtain Figs. 13 and 14.

Appendix C. Results for the atmospheric angle

For completeness in Fig. 18 we give $N_\sigma \equiv \sqrt{\chi^2}$ as a function of $\sin^2\theta_{23}$. The best fit values and the 3σ regions are summarised in Table 10.

References

[1] K. Nakamura, S.T. Petcov, in K.A. Olive, et al., Particle Data Group, Chin. Phys. C 38 (2014) 090001.
[2] S.K. Agarwalla, et al., J. High Energy Phys. 1405 (2014) 094;
    C. Adams, et al., arXiv:1307.7335 [hep-ex];
    A. de Gouvea, et al., arXiv:1310.4340 [hep-ex].
[3] N. Cabibbo, Phys. Lett. B 72 (1978) 333.

 [4] S.M. Bilenky, J. Hosek, S.T. Petcov, Phys. Lett. B 94 (1980) 495.
 [5] S.M. Bilenky, S.T. Petcov, Rev. Mod. Phys. 59 (1987) 671.
 [6] S.M. Bilenky, S. Pascoli, S.T. Petcov, Phys. Rev. D 64 (2001) 053010;
     S.T. Petcov, Phys. Scr. T 121 (2005) 94.
 [7] W. Rodejohann, Int. J. Mod. Phys. E 20 (2011) 1833.
 [8] P. Langacker, et al., Nucl. Phys. B 282 (1987) 589.
 [9] S. Pascoli, S.T. Petcov, A. Riotto, Phys. Rev. D 75 (2007) 083511.
[10] S. Pascoli, S.T. Petcov, A. Riotto, Nucl. Phys. B 774 (2007) 1.
[11] F. Capozzi, et al., Phys. Rev. D 89 (2014) 093018.
[12] M.C. Gonzalez-Garcia, M. Maltoni, T. Schwetz, J. High Energy Phys. 1411 (2014) 052.
[13] D. Marzocca, S.T. Petcov, A. Romanino, M.C. Sevilla, J. High Energy Phys. 1305 (2013) 073.
[14] S.T. Petcov, Nucl. Phys. B 892 (2015) 400.
[15] S. Antusch, S.F. King, Phys. Lett. B 631 (2005) 42.
[16] S.F. King, J. High Energy Phys. 0508 (2005) 105.
[17] S.F. King, et al., New J. Phys. 16 (2014) 045018.
[18] S.F. King, C. Luhn, Rep. Progr. Phys. 76 (2013) 056201.
[19] P.F. Harrison, D.H. Perkins, W.G. Scott, Phys. Lett. B 530 (2002) 167;
     P.F. Harrison, W.G. Scott, Phys. Lett. B 535 (2002) 163;
     Z.Z. Xing, Phys. Lett. B 533 (2002) 85;
     X.G. He, A. Zee, Phys. Lett. B 560 (2003) 87;
     see also L. Wolfenstein, Phys. Rev. D 18 (1978) 958.
[20] S.T. Petcov, Phys. Lett. B 110 (1982) 245.
[21] F. Vissani, arXiv:hep-ph/9708483;
     V.D. Barger, S. Pakvasa, T.J. Weiler, K. Whisnant, Phys. Lett. B 437 (1998) 107;
     A.J. Baltz, A.S. Goldhaber, M. Goldhaber, Phys. Rev. Lett. 81 (1998) 5730.
[22] L.L. Everett, A.J. Stuart, Phys. Rev. D 79 (2009) 085005.
[23] Y. Kajiyama, M. Raidal, A. Strumia, Phys. Rev. D 76 (2007) 117301.
[24] W. Rodejohann, Phys. Lett. B 671 (2009) 267;
     A. Adulpravitchai, A. Blum, W. Rodejohann, New J. Phys. 11 (2009) 063026.
[25] C.H. Albright, A. Dueck, W. Rodejohann, Eur. Phys. J. C 70 (2010) 1099.
[26] J.E. Kim, M.S. Seo, J. High Energy Phys. 1102 (2011) 097.
[27] I. Girardi, A. Meroni, S.T. Petcov, M. Spinrath, J. High Energy Phys. 1402 (2014) 050.
[28] M.C. Chen, K.T. Mahanthappa, Phys. Lett. B 681 (2009) 444;
     M.C. Chen, J. Huang, K.T. Mahanthappa, A.M. Wijangco, J. High Energy Phys. 1310 (2013) 112.
[29] P.H. Frampton, S.T. Petcov, W. Rodejohann, Nucl. Phys. B 687 (2004) 31.
[30] D. Marzocca, S.T. Petcov, A. Romanino, M. Spinrath, J. High Energy Phys. 11 (2011) 009.
[31] S. Antusch, V. Maurer, Phys. Rev. D 84 (2011) 117301;
     A. Meroni, S.T. Petcov, M. Spinrath, Phys. Rev. D 86 (2012) 113003;
     S. Antusch, C. Gross, V. Maurer, C. Sluka, Nucl. Phys. B 866 (2013) 255.
[32] C.H. Albright, M.C. Chen, Phys. Rev. D 74 (2006) 113006.
[33] W. Chao, Y.j. Zheng, J. High Energy Phys. 1302 (2013) 044.
[34] C. Giunti, M. Tanimoto, Phys. Rev. D 66 (2002) 053013, and Phys. Rev. D 66 (2002) 113006.
[35] A. Romanino, Phys. Rev. D 70 (2004) 013003.
[36] Y. Shimizu, M. Tanimoto, arXiv:1405.1521 [hep-ph].
[37] L.J. Hall, G.G. Ross, J. High Energy Phys. 1311 (2013) 091;
     Z. Liu, Y.L. Wu, Phys. Lett. B 733 (2014) 226;
     S.K. Garg, S. Gupta, J. High Energy Phys. 1310 (2013) 128.
[38] J. Gehrlein, J.P. Oppermann, D. Schäfer, M. Spinrath, Nucl. Phys. B 890 (2015) 539.
[39] S.F. King, T. Neder, A.J. Stuart, Phys. Lett. B 726 (2013) 312.
[40] C. Hagedorn, A. Meroni, E. Molinaro, Nucl. Phys. B 891 (2015) 499.
[41] C. Luhn, Nucl. Phys. B 875 (2013) 80.
[42] G. Altarelli, et al., J. High Energy Phys. 1208 (2012) 021;
     G. Altarelli, F. Feruglio, L. Merlo, Fortschr. Phys. 61 (2013) 507;
     F. Bazzocchi, L. Merlo, Fortschr. Phys. 61 (2013) 571.
[43] S. Antusch, et al., Nucl. Phys. B 674 (2003) 401;
     J.A. Casas, et al., Nucl. Phys. B 573 (2000) 652;

P.H. Chankowski, Z. Pluciennik, Phys. Lett. B 316 (1993) 312;
K.S. Babu, C.N. Leung, J. Pantaleone, Phys. Lett. B 319 (1993) 191.
[44] S.T. Petcov, T. Shindou, Y. Takanishi, Nucl. Phys. B 738 (2006) 219.
[45] G. Altarelli, F. Feruglio, I. Masina, Nucl. Phys. B 689 (2004) 157;
I. Masina, Phys. Lett. B 633 (2006) 134.
[46] K.A. Hochmuth, S.T. Petcov, W. Rodejohann, Phys. Lett. B 654 (2007) 177.
[47] P.I. Krastev, S.T. Petcov, Phys. Lett. B 205 (1988) 84.
[48] Y. Wang, PoS Neutel 2013 (2013) 030.
[49] P. Coloma, H. Minakata, S.J. Parke, Phys. Rev. D 90 (9) (2014) 093003.